HHS Public Access

Author manuscript

J Mol Cell Cardiol. Author manuscript; available in PMC 2020 December 01.

Published in final edited form as:

J Mol Cell Cardiol. 2019 December ; 137: 93–106. doi:10.1016/j.yjmcc.2019.09.013.

Metabolic regulation of Kv channels and cardiac repolarization by Kvβ2 subunits

Peter J. Kilfoil[1,†], **Kalyan C. Chapalamadugu**[2,†], **Xuemei Hu**[1], **Deqing Zhang**[1], **Frank J. Raucci Jr.**[1], **Jared Tur**[2], **Kenneth R. Brittian**[1], **Steven P. Jones**[1], **Aruni Bhatnagar**[1], **Srinivas M. Tipparaju**[2,*], **Matthew A. Nystoriak**[1,*]

[1]Department of Medicine, Christina Lee Brown Envirome Institute, and Diabetes and Obesity Center, University of Louisville, Louisville, KY

[2]Department of Pharmaceutical Sciences, Taneja College of Pharmacy, University of South Florida, Tampa, FL

Abstract

Voltage-gated potassium (Kv) channels control myocardial repolarization. Pore-forming Kvα proteins associate with intracellular Kvβ subunits, which bind pyridine nucleotides with high affinity and differentially regulate channel trafficking, plasmalemmal localization and gating properties. Nevertheless, it is unclear how Kvβ subunits regulate myocardial K^+ currents and repolarization. Here, we tested the hypothesis that Kvβ2 subunits regulate the expression of myocardial Kv channels and confer redox sensitivity to Kv current and cardiac repolarization. Co-immunoprecipitation and *in situ* proximity ligation showed that in cardiac myocytes, Kvβ2 interacts with Kv1.4, Kv1.5, Kv4.2, and Kv4.3. Cardiac myocytes from mice lacking *Kcnab2* ($Kv\beta2^{-/-}$) had smaller cross sectional areas, reduced sarcolemmal abundance of Kvα binding partners, reduced I_{to}, $I_{K,slow1}$, and $I_{K,slow2}$ densities, and prolonged action potential duration compared with myocytes from wild type mice. These differences in $Kv\beta2^{-/-}$ mice were associated with greater P wave duration and QT interval in electrocardiograms, and lower ejection fraction, fractional shortening, and left ventricular mass in echocardiographic and morphological assessments. Direct intracellular dialysis with a high NAD(P)H:$NAD(P)^+$ accelerated Kv inactivation in wild type, but not $Kv\beta2^{-/-}$ myocytes. Furthermore, elevated extracellular levels of lactate increased $[NADH]_i$ and prolonged action potential duration in wild type cardiac myocytes and perfused wild type, but not $Kv\beta2^{-/-}$, hearts. Taken together, these results suggest that Kvβ2 regulates myocardial electrical activity by supporting the functional expression of proteins that

[*]**To whom correspondence should be addressed:** Matthew A. Nystoriak, Diabetes and Obesity Center, Delia Baxter Bldg., 580 S. Preston St., Rm 421B, University of Louisville, Louisville, KY, 40202 (matthew.nystoriak@louisville.edu, Tel. 502-852-6024, Fax. 502-853-3663); Srinivas M. Tipparaju, Department of Pharmaceutical Sciences, 12901 Bruce B. Downs Blvd. MDC030, Taneja College of Pharmacy, University of South Florida, Tampa, FL, 33612, (stippara@usf.edu, Tel. 813-974-7195, Fax. 813-905-9885).
[†]These authors contributed equally to the work.

Disclosures

None.

generate I_{to} and $I_{K,slow}$, and imparting redox and metabolic sensitivity to Kv channels, thereby coupling cardiac repolarization to myocyte metabolism.

Keywords

heart; NAD; arrhythmia; metabolism; redox

Introduction

The mammalian heart depends upon the coordinated function of voltage-gated K^+ (Kv) channels for precise control of electrical activity and myocardial contractility. In cardiac myocytes, several types of Kv channels conduct outward K^+ currents that collectively determine the amplitude and the duration of the action potential [1, 2]. The importance of proper Kv channel function to cardiac electrophysiology is underscored by the robust association of human arrhythmias with gain-of-function and loss-of-function mutations in Kv channel encoding genes [3, 4], and deficits in ventricular repolarization in mice with genetic ablation of Kv subunits [5–7]. These associations support the notion that the regulation of Kv channel function is important for normal repolarization of the cardiac action potential and that even small alterations in Kv conductance could profoundly impact cardiac repolarization and increase the propensity for developing arrhythmias.

Members of the Kv family are multi-protein complexes consisting of pore-forming heterotetramers that variably associate with intracellular auxiliary subunits, such as Kvβ, KChAP, KChIP and MinK, which differentially modulate Kv gating [8]. Members of the *Shaker* (Kv1) and *Shal* (Kv4) families contribute to both early and late phases of myocyte repolarization and are known to associate with Kvβ subunits [9, 10]. Studies in neurons and heterologous expression systems have shown that the Kvβ proteins (Kvβ1–3) bind to the intracellular domain of the channel pore-forming subunits and regulate Kv trafficking and membrane expression [11–13], subcellular localization [14, 15], and channel gating [16–19]. Previous work has shown that Kvβ1 and Kvβ3 subunits impart rapid N-type inactivation to otherwise non-inactivating members of the Kv1 family, whereas Kvβ2 lacks the N-terminal domain responsible for rapid inactivation, and therefore, unlike Kvβ1/3, does not impart N-type inactivation to Kv1 channels. Nonetheless co-expression of Kvβ2 with Kv channels accelerates inactivation and shifts the voltage-dependence of the activation of Kv1.4 and Kv1.5 channels [8].

Mammalian Kvβ proteins are members of the aldo-keto reductase (AKR) superfamily (AKR6A), which are functional oxidoreductases that bind pyridine nucleotides with K_d values in the low micromolar range [20, 21] and catalyze the reduction of a wide range of carbonyl substrates [22–24]. Although the physiological significance of the catalytic function of Kvβ proteins remains unclear, the redox status of the pyridine nucleotide bound to Kvβ regulates Kvα/β interactions and gating. Hence, regulation of Kv gating by the redox status of pyridine nucleotides bound to Kvβ may facilitate communication between intermediary metabolism and membrane excitability. Nevertheless, the physiological role of Kvβ in regulating native Kv channels in the heart remains unclear.

The adult mouse ventricle expresses Kvβ1.1, Kvβ1.2, and Kvβ2 proteins; however, in ventricular lysates, Kvβ1 predominantly co-immunoprecipitates with Kv4.2 and Kv4.3 proteins, rather than members of the Kv1 family [25]. Loss of Kvβ1 reduces sarcolemmal abundance of Kv4.3 and suppresses $I_{to,fast}$, while the functional expression of Kv1.5 is not affected. However, the myocardial role of Kvβ2 remains obscure. A recent study identified several rare genetic variants of the *KCNAB2* gene, which encodes Kvβ2, in a subset of patients exhibiting electrocardiographic features of Brugada syndrome [26]. Two variants (R12Q and L13F) were found to significantly increase K^+ current density upon coexpression with Kv4.3, underscoring the potential physiological and clinical significance of Kvβ2 in supporting functional I_K in cardiac myocytes. Nevertheless, the binding partners of Kvβ2 have not been identified and it remains unclear how the expression of Kvβ2 modifies Kv currents in the heart. Hence, in the current study, we tested the hypothesis that Kvβ2 binds to native cardiac Kv1 and Kv4 proteins and regulates the currents mediated by these channels. Moreover, using genetically engineered mice lacking *Kcnab2*, we tested whether ablation of Kvβ2 impacts the pyridine nucleotide sensitivity of cardiac repolarization.

Methods

Ethical approval

All animal procedures were conducted as approved by Institutional Animal Care and Use Committees at the University of Louisville and the University of South Florida, in accordance with guidelines set by the National Institutes of Health.

Animals and isolation of cardiac myocytes

Mice in which the *Kcnab2* gene was ablated ($Kv\beta2^{-/-}$; obtained from investigators in [9, 27]) and strain-matched wild type (mixed C57BL/6 × 129/SvEv) mice (25–30 g body mass) were bred in house and fed normal rodent chow *ad libitum*. Male mice, 12–24 weeks of age, were administered heparin (10,000 U/kg; I.P.) prior to euthanasia by sodium pentobarbital (150 mg/kg; I.P.). Hearts were excised and left ventricular and septal myocytes were isolated as previously described [28]. Briefly, hearts were perfused with Tyrode's solution containing (in mM): 126 NaCl, 4.4 KCl, 1 $MgCl_2$, 18 $NaHCO_3$, 4 HEPES, 11 glucose, 20 2,3-butanedione monoxime, and 30 taurine (pH 7.4), followed by digestion with Liberase TH enzyme blend (0.28 mg/mL; Roche, Indianapolis, IN) for ~8 min. After perfusion, the hearts were minced using fine forceps, followed by gentle trituration. Cell suspensions were then filtered through 100 μm pore mesh to remove undigested tissue, and isolated myocytes were allowed to settle by gravity (20 min). Myocytes were then sequentially resuspended and pelleted in Tyrode's solution (5x) containing increasing $[Ca^{2+}]_o$ (up to 0.5 mM). Cells were kept at 4°C, and used within 12 h of isolation.

Echocardiography

Transthoracic echocardiography data were acquired in a blinded manner using a Vevo 770 echocardiography system (VisualSonics), as described previously [29–31]. For the procedure, the mice were anesthetized (2.0% isoflurane induction, 1.0–1.5% maintenance) and placed chest up on an examination board. Body temperature was monitored continuously and maintained at 36.5–37.5 °C with a rectal thermometer interfaced with a

servo-controlled heat lamp. Two-dimensional images of the parasternal long axis were captured at 100 fps using a 707-B (30 MHz) scan head. The same anatomical position was used for M-mode imaging. All echocardiographic data were obtained from at least five independent cardiac cycles per experiment.

Electrocardiography

Mice were anesthetized with isoflurane (1–2%) and telemetric transmitters were implanted in the abdominal cavity with one lead placed under the right clavicle and the other at the left side of the xiphoid cartilage. ECG recordings were acquired three days after surgery. Data were sampled at 1000 Hz using DSI software (Dataquest A.R.T. System) and analyzed using LabChart 7.2 software (ADInstruments, Colorado Springs, CO). The T wave was fixed at the time of return to isoelectric baseline and intraventricular conduction (QRS) and repolarization (QT and QTc calculated using Bazett's formula: $QTc = QT/RR^{1/2}$) were estimated as reported previously [32].

Immunofluorescence, proximity ligation, and imaging

Isolated cardiac myocytes were fixed in 3% paraformaldehyde and phosphate buffered saline (PBS; pH 7.4) for 10 min and washed in PBS (3×; 15 min each). Fixed cells were adhered to poly-lysine coated glass microscope slides using a Cytospin 4 Cytocentrifuge (Thermo Fisher Scientific; 300 rpm, 5 min). Centrifugation using this protocol had no observable effect on the morphology of fixed cells. After adhering to slides, the cells were permeabilized by incubation in PBS containing 0.1% Triton-X 100 for 9 min at room temperature and washed 3× in PBS. Non-specific antibody binding sites were blocked by incubating cells in PBS containing 1% BSA, 300 mM glycine, and 0.1% Tween 20 (30 min, room temperature). Cells were then incubated for 1 h at room temperature in blocking solution containing primary antibodies against Kvβ2 (Aviva Bio Systems; ARP37678_T100; 20 μg/ml) [33] or against an extracellular epitope of Kv1.5 (Alomone; APC-150; 3.2 μg/ml) [34]. After washing, the cells were incubated in Alexa Fluor 647-conjugated goat anti-rabbit secondary antibody (Invitrogen; 0.5 μg/ml; 45 min, room temperature).

A separate set of slides were used to detect Kv protein-protein interactions using an *in situ* proximity ligation (PLA) assay, as previously described [35, 36]. Briefly, fixed myocytes were permeabilized with 0.1% Triton X-100 (10 min, room temperature) and a Duolink *in situ* proximity ligation (PLA) kit (Sigma Aldrich) was used to detect proximity between Kv subunits in complex per manufacturer's instructions. After blocking non-specific binding with Duolink blocking solution, the cells were incubated overnight in primary antibodies against Kvβ2 (Aviva Bio Systems, as above; Neuromab, K17/70), Kv1.4 (NeuroMab, L13/31), Kv1.5 (NeuroMab, K7/45), Kv2.1 (NeuroMab, K80/21), Kv4.2 (NeuroMab, L28/4), and Kv4.3 (Alomone, APC-017). As a control, the cells were incubated only with antibodies against Kvβ2. Antibodies bound to target proteins were detected with oligonucleotide-conjugated secondary antibodies (anti-mouse MINUS; anti-rabbit PLUS). Oligonucleotides were joined to form circular DNA by incubating in a ligation solution including probe-specific oligonucleotides and ligase, followed by rolling circle amplification and fluorophore labelling of a concatemeric product at sites of protein-protein proximity. Slides for immunostaining and PLA experiments were counterstained in SlowFade Gold

with DAPI mounting medium and stored in the dark at 4°C until imaging. The specificity of antibodies to detect Kvβ2 used in immunofluorescence and PLA experiments was tested using myocytes from Kvβ2$^{-/-}$ mice (see Figs. 1C, 2B). In addition, detection of target proteins by anti-Kv primary antibodies was verified by comparison of fluorescent signals between transfected (expression vectors containing mouse Kvβ2, Kv1.4, Kv1.5, Kv2.1, Kv4.2, or Kv4.3 with either mCherry or EGFP reporters) versus untransfected COS-7 cells labeled for respective proteins (see Figure S1). In control experiments, to test the specificity of secondary antibodies, primary antibodies were omitted from the procedure.

For immunofluorescence experiments, cells were imaged with a Nikon A1 confocal microscopy system coupled with a 60× oil-immersion objective lens (NA = 1.4). Identical laser power, photomultiplier gain, and pinhole size were used to capture images of cells for each experimental group. For PLA experiments, images were captured in a z-series (1 μm steps) using a Nikon eclipse Ti epifluorescence microscope. Punctate sites of fluorescence were counted from flattened z-projection images using the z-project and particle analyzer functions in FIJI software (NIH).

Histology

Hearts were excised, flushed with 1 M KCl in PBS and a 1 mm thick transverse section from the mid-ventricular region was fixed in 10% formalin (24 h), washed with 70% ethanol, embedded in paraffin and sections (4μm) were cut and placed onto slides. Heart sections were stained with either hematoxylin and eosin (H & E), or Alexa Fluor 555-conjugated wheat germ agglutinin membrane stain (WGA; Thermo Fisher Scientific) and 4'6-diamidino-2-phenylindole nuclear stain (DAPI, Thermo Fisher Scientific). Images were acquired using a Nikon Eclipse Ti epifluorescence microscope and cardiac myocyte cross sectional area was measured in left and right ventricular (epicardial and endocardial) and septal regions (area values of 50 myocytes were pooled for each region of each heart) using FIJI software (NIH).

Immunoblotting and immunoprecipitation

Left ventricular tissue lysates were prepared by homogenization in T-PER Tissue Protein Extraction Reagent (Thermo Fisher Scientific) supplemented with 10 mM DTT, 10 mM protease inhibitor (Sigma), and 10 mM phosphatase inhibitor cocktails II (Sigma). Tissue lysate was then centrifuged (10,000×*g*, 10 min, 4°C) and the supernatant was collected. In some experiments, differential centrifugation was used to prepare membrane-enriched fractions from heart lysates as described previously [37]. Briefly, frozen ventricular tissue was thawed on ice and homogenized in 500 μl of lysis buffer solution (225 mM mannitol, 75 mM sucrose, 1 mM EGTA, 30 mM Tris-HCl, with protease inhibitor cocktail, pH 7.4). Nuclear debris and undisrupted tissue were removed by two sequential centrifugations of the homogenate at 1000×*g* for 10 min with pooling of the low-speed supernatant. The pooled low-speed supernatants were then centrifuged at 100,000×*g* for 1 h. The high-speed supernatants were saved for use as a control and resulting pellets were washed in 200 μl of a solution containing (50 mM Tris, 1mM EDTA, 2% Sarkosyl) until completely dissolved. Total protein (50–100 μg) was loaded onto a 10% polyacrylamide gel (Bio-Rad) and separated by SDS-PAGE before being transferred onto polyvinylidene fluoride (PVDF)

membranes. Membranes were stained with Ponceau-S to verify uniform protein transfer, washed in Tris-buffered saline containing 0.1% Tween-20 (TBS-t) and blocked for 45 min in TBS-t containing 5% non-fat milk. Blots were probed overnight at 4°C with anti-Kv1.4 (NeuroMab; L13/31, 10 μg/ml) [38], anti-Kv1.5 (Alomone; APC-004; 6 μg/ml) [39, 40], anti-Kv2.1 (NeuroMab; 80/21,10 μg/ml) [41], anti-Kv4.2 (NeuroMab; L28/4, 10 μg/ml) [39, 42], anti-Kv4.3 (Alomone; APC-017, 4 μg/ml) [43], anti-Kvβ2 (NeuroMab; K17/70, 10 μg/ml) [44], anti-Kvβ1.1 (NeuroMab; K9/40; 10 μg/ml) [39], anti-KChIP2 (Abcam; ab99041, 10 μg/ml) [45], anti-pan cadherin (Santa Cruz; sc-1499, 1 μg/ml), and anti-GAPDH (Millipore; MAB374; 1 μg/ml). After washing (5×, 10 min each), the blots were incubated in HRP-conjugated goat anti-rabbit, rabbit anti-mouse (Cell Signaling; 0.7 μg/ml), or donkey anti-goat (Thermo Fisher Scientific, PA1–28664) secondary antibodies in TBS-t containing 5% non-fat milk (1 h, room temperature). After the final washing step (5×, 10 min each), HRP was detected with ECL reagent (Thermo Fisher Scientific) and a myECL imager (Thermo Fisher Scientific).

For co-immunoprecipitation experiments, 50 μl of protein G-coated magnetic beads (Life Technologies) were incubated (4°C, overnight with nutation) with 10 μg of anti-Kvβ2 (NeuroMab; K17/70) primary antibodies in 200 μl of PBS with 0.01% Tween-20 (PBS-t). Antibodies were cross-linked to magnetic beads by washing with PBS containing 50 mM sodium borate (pH 9) followed by incubation (30 min, room temperature with nutation) in PBS containing 50 mM sodium borate and 25 mM dimethyl pimelimidate. The beads were then resuspended in ethanolamine, washed with PBS-t (3×), and incubated with lysates (4°C, overnight with nutation). The supernatants were removed and saved. Beads were resuspended in 1:5 SDS loading buffer with 150 mM DTT in PBS plus 0.01% Tween-20 and then incubated at 70°C for 10 min. The supernatants were removed and incubated at 100°C for 10 min. Eluted samples were then fractionated and immunoblotted as described above. The specificity of primary antibodies used to detect Kvβ2 in immunoblotting experiments was verified by lack of immunoreactive bands in heart lysates from $Kv\beta2^{-/-}$ mice (see Figures 1B, 2B). Additionally, detection of target Kv proteins by anti-Kv primary antibodies at expected molecular weights was verified by separate Western blot experiments comparing immunoreactivity in lysates from untransfected and transfected COS-7 cells expressing genes of interest (Figure S2).

Patch clamp electrophysiology

Cardiac myocytes isolated from the left ventricular apical and septal regions were used for electrophysiological recordings. Electrical activity was recorded using the conventional whole-cell configuration of the patch clamp technique in voltage clamp or current clamp mode using an Axopatch 200B patch clamp amplifier (Axon Instruments). For voltage-clamp experiments, cells were patched using borosilicate glass pipettes (1B150F-4 and TW150F-4, World Precision Instruments) pulled using a P-87 micropipette puller (Sutter Instruments) to a resistance of 2–4 MΩ when filled with a pipette solution containing (in mM): 100 K-aspartate, 30 KCl, 1 $MgCl_2$, 5 HEPES, 5 EGTA, 5 Mg-ATP, 5 NaCl (pH 7.2, adjusted with KOH). In these experiments, series resistance was electronically compensated by >80%. For current clamp experiments, pipette resistance was 7–10 MΩ when filled with the same pipette solution. Cardiac myocytes were placed in a 0.25 ml recording chamber

(RC-26, Warner Instruments) and perfused with an external solution containing (in mM): 135 NaCl, 1.1 $MgCl_2$, 1.8 $CaCl_2$, 5.4 KCl, 10 HEPES, 5.5 glucose (pH 7.4, adjusted with NaOH). For recording Kv currents, the cells were held at −80 mV and then subjected to a pre-pulse of −40 mV (50 ms) to inactivate the sodium current, followed by depolarization to +50 mV (5 s). Unless otherwise indicated, patch clamp recordings were performed at room temperature.

For experiments testing the effects of lactate, the perforated whole-cell patch configuration was used. For this, amphotericin B (Sigma-Aldrich) was dissolved in DMSO and diluted in pipette internal solution to a final concentration of 250 μg/ml. After forming a GΩ seal, the cells were equilibrated for ~5 min to obtain a stable reading of membrane potential (~ −75 mV). Upon stabilization, action potentials were elicited via small current injections of 0.8–1.0 nA lasting 2 ms at a frequency of 1 Hz. Action potentials were recorded for 4 min and used as baseline control values. The cells were then perfused with buffer containing 10 mM sodium lactate, during which time the action potentials were continuously recorded [46].

Patch clamp data were analyzed using Clampfit 9 (Axon Instruments). Peak currents were defined as the maximal K^+ current reached over the period of depolarization. The amplitudes and inactivation time constants of outward currents were best-fits of a tri-exponential function obtained by using the Levenberg-Marquardt (SP) iterative function in Clampfit analysis software. Only fittings with a correlation coefficient ≥0.98 were used for analysis. Peak and component amplitudes were normalized to cell capacitance and expressed as pA/pF. Cell membrane capacitance was calculated immediately upon reaching whole cell configuration by Clampfit through integration of transient currents evoked by a 10 mV voltage step from the holding potential. Mouse ventricular action potentials were simulated using a mathematical model described previously [47]. Parameters were adjusted so that each current magnitude reflected current densities of $I_{to,fast}$, $I_{to,slow}$, $I_{K,slow1}$ and $I_{K,slow2}$ measured on voltage clamp recordings. Cellular action potential recordings were analyzed using Excel to calculate the resting membrane potential, action potential amplitude, dV/dt_{max}, and action potential durations at 20% (APD_{20}), 50% (APD_{50}) and 90% (APD_{90}) repolarization. Action potentials recorded after 30 s of pacing at 1 Hz were used for comparison. APD values in the presence of lactate are expressed as relative to control baseline values.

Cardiac monophasic action potentials (MAP) recordings

Hearts from wild type and Kvβ2$^{-/-}$ mice were isolated and left ventricular epicardial action potentials (AP) were recorded *ex vivo* as reported previously [39, 46]. Bilateral thoracotomies were performed to retract the chest and hearts were isolated and arrested in ice-cold Krebs-Henseleit buffer of the following composition (in mM): 119 NaCl, 25 $NaHCO_3$, 4 KCl, 1.2 KH_2PO_4, 1 $MgCl_2$, 1.8 $CaCl_2$, 10 D-glucose, and 2 sodium pyruvate (pH 7.4, adjusted with NaOH). After removing the surrounding tissue, the aortae were secured onto a cannula (1.3 mm diameter) with 1–0 silk suture and the hearts were mounted on a Langendorff perfusion apparatus (Harvard Apparatus). Hearts were perfused at a flow rate of 2 ml/min with Krebs-Henseleit buffer aerated with 95% O_2/5% CO_2 (37°C). Monophasic action potentials from the left ventricular (LV) epicardial surface were recorded

using a contact electrode (Harvard Apparatus) connected to an 8-channel PowerLab amplifier and data acquisition system (AD Instruments). Hearts were equilibrated for 10 min before collecting MAP traces to ensure stable baseline recordings. Following equilibration, the hearts were perfused (10 min) with Krebs-Henseleit buffer containing 20 mM L-lactate, followed by buffer containing 20 mM pyruvate (15 min) [39]. Data were continuously acquired at a sampling frequency of 1 kHz and analyzed offline using LabChart 7.2 software (AD Instruments).

Measurements of intracellular NADH

NADH levels in whole hearts were measured as reported previously [32]. Hearts were freeze-clamped using Wollenberger forceps and stored at −80 °C until use. Frozen hearts were pulverized and cardiac $[NADH]_i$ was measured in ~20 mg of powdered tissue using an EnzyChrom NAD/NADH assay Kit (Bioassay Systems) according to manufacturer's instructions. Total $[NADH]_i$ was calculated for each sample and normalized to total protein concentration determined using a Pierce 660 nm Protein Assay (Thermo Fisher Scientific). Data are expressed relative to baseline control (i.e., minus lactate/pyruvate) group.

Statistics

Data, presented as mean ± SEM, were analyzed using Microsoft Excel or GraphPad Prism software using paired or unpaired Student's t-test and Wilcoxon non-parametric signed rank test for paired experiments that were normalized to baseline control values. One-way analysis of variance or non-parametric tests with appropriate post-hoc tests were used for comparison of multiple groups. P values <0.05 were considered significant.

Results

Myocardial Kvβ2 associates with Kv1 and Kv4 channels

In general, the Kvβ proteins are known to assemble with channels of the Kv1 and Kv4 family, however, the specific Kvα subunits that associate with Kvβ2 in the heart have not been identified. Consistent with previous work demonstrating expression of Kvβ subunits in the myocardium [25, 48], we detected Kvβ2 protein in whole heart homogenates from wild type animals (Figure 1A, *lane 1*). Upon immunoprecipitation of Kvβ2, we detected immunoreactive bands corresponding to Kv1.4, Kv1.5, Kv4.2, and Kv4.3 proteins (Figure 1A, *lane 2*). No immunoreactive bands were observed at the molecular weights expected for these Kv subunits when mouse IgG was substituted on immunoprecipitation beads for anti-Kvβ2 primary antibody (Figure 1A, *lane 3*). Moreover, no bands were observed at the molecular weight predicted for Kvβ2 (37 kDa, see Fig. S2H) in immunoprecipitates from mice in which the gene encoding Kvβ2 (*Kcnab2*) was ablated (Figure 1B), indicating specific immunoprecipitation of Kvβ2.

To identify Kvβ2/Kvα interactions in isolated cardiac myocytes, we performed a series of *in situ* proximity ligation assays (PLA). This assay detects spatial proximity (≤40 nm) between target proteins in their native cellular environment, and has been shown to be useful for the identification and quantitation of protein-protein interactions in isolated cells, including those of native ion channel complexes in cardiovascular tissues [35, 36, 49]. Proximity

ligation experiments in which the cells were probed with both mouse and rabbit-derived primary antibodies against Kvβ2 identified discrete fluorescent punctae within single cardiac myocytes from wild type animals, but not in myocytes isolated from Kvβ2$^{-/-}$ animals, suggesting specificity of the assay for Kvβ2 and its interacting Kvα subunits (Figure 1C). Consistent with co-immunoprecipitation data, we observed a significant increase in the number of fluorescent punctae when cells were co-labeled with antibodies targeting Kvβ2 and either Kv1.4, Kv1.5, Kv4.2 or Kv4.3 when compared with cells that were labeled with anti-Kvβ2 only (Figure 1D–E; P<0.0001). Moreover, PLA signal in cells co-labelled for Kvβ2 and Kv2.1, which is not a purported binding partner of the Kvβ proteins, was similar to that of cells labelled for Kvβ2 alone (P = 0.978). Together, these data identify Kv1.4, Kv1.5, Kv4.2, and Kv4.3 as binding partners of Kvβ2 subunits in cardiac myocytes.

To determine the physiological role of Kvβ2 subunits, we examined Kvβ2$^{-/-}$ mice. As previously reported, Kvβ2$^{-/-}$ mice are viable into adulthood [9]. Immunostaining for Kvβ2 and confocal imaging revealed that this subunit is abundant in the sarcolemma in wild type cardiac myocytes (Figure 2A). Western blot analyses of wild type and Kvβ2$^{-/-}$ hearts suggested that the loss of Kvβ2 does not lead to significant compensatory changes in the total protein abundance of other prominent Kv channel subunits, including Kv1.4, Kv1.5, Kv2.1, Kv4.2, Kv4.3, Kvβ1.1, Kvβ1.2, and KChIP2 (Figure 2B, C; p = 0.070 – 0.730).

In heterologous expression systems, Kvβ acts as a protein chaperone, which facilitates the surface expression of Kv channels [8, 13]. Hence, we examined whether loss of Kvβ2 would alter the surface expression of Kv1 and Kv4 proteins identified as binding partners in cardiac myocytes (Figure 1). For this, we isolated the sarcolemmal fraction from myocardial lysates using differential centrifugation. Membrane separation was confirmed by a lack of the sarcolemmal marker protein pan-cadherin in the cytosolic fraction (Figure 2D). Measurements of relative protein abundances by Western blot showed that even though there were no differences in total Kv1 and Kv4 proteins between wild type and Kvβ2$^{-/-}$ hearts (see Figure 2C), the abundances of membrane-associated Kv1.5, Kv4.2, and Kv4.3 were significantly reduced (P = 0.037, 0.034, and 0.003, respectively) in Kvβ2$^{-/-}$ hearts compared with wild type controls (Figure 2D–H). In addition, there was a trend in the data towards reduced sarcolemmal abundance of Kv1.4 in hearts from Kvβ2$^{-/-}$ amimals (P = 0.097) Reduced sarcolemmal expression was further confirmed for Kv1.5 by immunofluorescence experiments in non-permeabilized cardiac myocytes using primary antibodies that recognize an extracellular epitope on Kv1.5. Using this approach, we observed that Kv1.5-associated fluorescence was significantly lower in cardiac myocytes isolated from Kvβ2$^{-/-}$ mice than that in myocytes from wild type mice (Figure S3A–C). Total fluorescence intensities associated with Kv1.5 were not different between permeabilized cardiac myocytes from wild type and Kvβ2$^{-/-}$ mice (Figure S3D, E). Together, these data indicate that in cardiac myocytes, Kvβ2 promotes the sarcolemmal expression of Kv1 and Kv4 channels.

Role of Kvβ2 in regulating cardiac Kv current density

We next determined the role of Kvβ2 subunits in the regulation of Kv-mediated currents by comparing the magnitude of K^+ current densities and inactivation rate of currents in wild type and Kvβ2$^{-/-}$ myocytes. The I-V relationships for K^+ currents in wild type and Kvβ2$^{-/-}$

myocytes are shown in Figure 3A. When compared with wild type myocytes, we found that the peak Kv current density was significantly lower in myocytes from Kvβ2$^{-/-}$ animals (e.g., 60 mV, P = 0.035). To assess the impact of Kvβ2 ablation on Kv current, we used a tri-exponential function to dissect composite currents that were elicited by a 50 mV depolarizing stimulus from a holding potential of −80 mV into three distinct components with different inactivation time constants [50]. This analysis showed that the magnitude of Kv current associated with the rapidly inactivating (I_{to}), intermediate inactivating ($I_{K,slow1}$), and slowly inactivating ($I_{K,slow2}$) exponential components was significantly reduced in cardiomyocytes from Kvβ2$^{-/-}$ animals, when compared with respective kinetic components of K^+ currents recorded from wild type myocytes (Figure 3B and C, Table S1; P = 0.005, 0.048, and 0.040, respectively). Values of inactivation time constants associated with each exponential term were similar between groups (Table S1).

Because Kv currents are key mediators of repolarization, we next examined whether a reduction in Kv current density, due to the loss of Kvβ2, was associated with prolongation of the action potential. Reductions in I_{to}, $I_{K,slow1}$, and $I_{K,slow2}$ (seen in Kvβ2$^{-/-}$ mice; Figure 4) delay myocyte repolarization in an established mathematical model [47] of the murine ventricular action potential (Figure 4A). To experimentally test the predictions of the model, we measured repolarization in cardiac myocytes as the time required for the return of membrane potential to 20, 50, and 90% of the resting membrane potential from the peak of the action potential waveform (APD_{20}, APD_{50}, and APD_{90}, respectively). We found that repolarization was significantly slower in myocytes isolated from Kvβ2$^{-/-}$ animals than in wild type myocytes, as evidenced by a significant increase at each APD examined (Figure 4B, C; $APD_{20,}$ P = 0.008; APD_{50}, P = 0.026; APD_{90}, P = 0.005). Other action potential parameters including upstroke velocity (dV/dt_{max}), resting membrane potential, and action potential amplitude were similar between groups (Table S1). These results suggest that the loss of Kvβ2 prolongs the action potential by suppressing repolarizing Kv currents.

To examine the role of Kvβ2 in cardiac repolarization further, we recorded cardiac action potentials from hearts perfused *ex vivo* in the Langendorff mode. Monophasic action potentials were recorded from the left ventricular epicardial surface of hearts from both wild type and Kvβ2$^{-/-}$ mice (Figure 4D). In agreement with findings in isolated myocytes, we found that APD_{20}, APD_{50}, and APD_{90} were significantly greater in hearts from Kvβ2$^{-/-}$ mice when compared with those from wild type mice (Figure 4E; P = 0.003, <0.0001, and 0.001, respectively). We tested whether changes in APD were associated with changes in ECG waveform in conscious mice. Figure 5F shows representative ECG waveforms recorded from wild type and Kvβ2$^{-/-}$ mice. Consistent with prolonged APD, we found significantly greater P duration and QT interval (QT and QTc) in Kvβ2$^{-/-}$ mice (Figure 4G–H). No significant differences were observed in RR interval (P = 0.155), heart rate (P = 0.145), PR interval (P = 0.198), or JT interval (P = 0.187) (Table S2). Taken together, these data indicate that Kvβ2 plays a functional role in enhancing the magnitude of cardiac myocyte Kv current density and thereby regulates the repolarization of the action potential.

Cardiac function and heart morphology in Kvβ2$^{-/-}$ mice

We next examined whether genetic ablation of Kvβ2 is associated with phenotypic changes in heart function or morphology. Echocardiographic data related to endocardial parameters, chamber diameter and wall dimensions for wild type and Kvβ2$^{-/-}$ mice are shown in Table S3. Echocardiographic measurements revealed a modest, yet statistically significant, reduction in fractional shortening and ejection fraction in Kvβ2$^{-/-}$ mice when compared with wild type mice. We also found that heart weight, normalized to tibia length, was significantly lower in Kvβ2$^{-/-}$ mice than in wild type mice (Figure 5A, B). This difference was attributed to reduced left ventricular mass in Kvβ2$^{-/-}$ mice as right ventricular mass was not different between the two groups (Figure 5C). In patch clamp experiments, left ventricular and septal myocytes had nominally reduced cell capacitance (Table S1), which did not reach statistical significance (P = 0.154); however, histological assessment of cardiac myocyte size in heart sections revealed significantly reduced myocyte cross sectional area in the left ventricular endocardial and septal regions in hearts from Kvβ2$^{-/-}$ mice, while the size of right ventricular and left ventricular epicardial myocytes was not different between groups (Figure 5D, E). These observations suggest that the expression of Kvβ2 subunits by cardiac myocytes regulates Kv currents as well as myocyte size, and may influence the contractile function of the heart.

Kvβ2 imparts sensitivity of cardiac $I_{K,slow}$ to the redox state of pyridine nucleotides

Heterologous co-expression of Kv1α and Kvβ generates Kv currents with inactivation rates that are differentially modified by oxidized and reduced pyridine nucleotides [17, 22, 51, 52]. Given that Kvβ proteins modulate Kv current density in cardiac myocytes (Figure 3 and see [25, 39]), we postulated that native cardiac Kv currents are sensitive to changes in the redox status of intracellular pyridine nucleotides, which may reflect altered metabolism during stress conditions such as ischemia and hypoxia. To test this hypothesis, K^+ currents were recorded using the whole-cell configuration of the patch clamp technique from isolated myocytes. To alter levels of intracellular pyridine nucleotides, myocytes were dialyzed with pipette solutions chosen to mimic the ratio of pyridine nucleotides in normoxic (i.e., high [NAD(P)$^+$]:[NAD(P)H]) or hypoxic (i.e., low [NAD(P)$^+$]:[NAD(P)H]) conditions [53, 54]. These ratios are listed in the inset in Figure 6A. After forming a gigaohm seal, the intracellular content of the myocyte was dialyzed by the pipette solution for ~5 min, after which, depolarization-evoked outward K^+ currents were recorded. Analysis of the data, using a multi-exponential function, indicated that in comparison with the normoxic ratios, the hypoxic levels of pyridine nucleotides increased the rate of inactivation of native Kv currents in myocytes from wild type mice (Figure 6A and B). Specifically, the time constants associated with the intermediate and slowly inactivating Kv currents, $I_{K,slow1}$ and $I_{K,slow2}$, respectively, were significantly lower in myocytes that were dialyzed with hypoxic ($I_{K,slow1}$ = 145.2 ± 11.6 ms; $I_{K,slow2}$ = 804.9 ± 99.1 ms) than normoxic levels of pyridine nucleotides ($I_{K,slow1}$ = 188.8 ± 6.1 ms; $I_{K,slow2}$ = 1319.3 ± 85.3 ms; Figure 6B–E). However, the rapidly inactivating component associated with the transient outward Kv current, I_{to}, was not statistically different (P = 0.160) between the hypoxic and normoxic groups. Note that Kv current density was similar between groups (normoxic: 95.0 ± 8.8 pA/pF; hypoxic: 89.9 ± 10.8 pA/pF; P = 0.957). Remarkably, changes in Kv inactivation evoked by hypoxic versus normoxic levels of pyridine nucleotides were abolished by the loss of Kvβ2 (Figure 6B–E).

Collectively, these data suggest that the Kv currents of cardiac myocytes are sensitive to changes in the redox state of pyridine nucleotides such that conditions increasing the NAD(P)H:$NAD(P)^+$ ratio enhance inactivation of slowly inactivating currents and that this effect requires Kvβ2.

Ablation of Kvβ2 prevents redox sensitivity of the cardiac action potential

To examine whether action potential repolarization was sensitive to redox changes secondary to changes in intermediary metabolism, we perfused isolated myocytes with 20 mM lactate to alter pyridine nucleotide redox ratio in favor of NADH over NAD^+ via the lactate dehydrogenase reaction [39, 55, 56]. Previous work has shown that at 20 mM extracellular lactate, the interconversion of lactate to pyruvate is near equilibrium, which correctly predicts an intracellular NAD^+/NADH ratio of ~45 [57]. To test the efficacy of this intervention in changing $[NADH]_i$ concentration, we perfused isolated hearts with lactate for 20 min, which led to a significant increase (~2-fold) in intracellular NADH levels (Figure 7A, *inset*). When isolated myocytes were perfused with the same concentration of lactate, there was a significant prolongation of the action potential (Figure 7A, B; APD_{20}, P = 0.006; APD_{50}, P = 0.015; APD_{90}, P = 0.181). Consistent with a predominant effect on repolarizing currents, there were no statistically significant effects of lactate perfusion on action potential amplitude (wild type: 127.9 ± 2.4 mV; $Kv\beta2^{-/-}$: 126.2 ± 2.3 mV; P = 0.051), resting membrane potential (wild type: −83.4 ± 2.1 mV; $Kv\beta2^{-/-}$: −83.1 ± 2.2 mV; P = 0.436), or dV/dt_{max} (wild type: 161.7 ± 20.1 mV/ms; $Kv\beta2^{-/-}$: 158.6 ± 21.3 mV/ms; P = 0.436). When taken together, these findings support the notion that metabolic conditions that favor a more reduced redox state of pyridine nucleotides prolong the action potential by accelerating Kv inactivation. This is consistent with the results of our previous experiments showing that an increase in intracellular NAD(P)H accelerates Kvβ-mediated inactivation of Kv currents [51, 52].

To address whether lactate also prolongs action potentials in the intact heart, we recorded monophasic action potentials from the left ventricular epicardial surface of perfused hearts under control conditions and after application of 20 mM lactate or 20 mM pyruvate to ensure that the NAD^+/NADH or lactate/pyruvate conversion was at equilibrium [57]. Representative action potentials recorded under each of these conditions are shown in Figure 7C. Consistent with observations in isolated cardiac myocytes (Figure 7A, B), action potential durations (APD_{20}, APD_{50}, APD_{90}) were significantly prolonged after the application of lactate (Figure 7C, D; APD_{20}, P = 0.041; APD_{50}, P = 0.026; APD_{90}, P = 0.025). Subsequent application of pyruvate, which conversely increases $[NAD^+]_i$, restored action potential duration to control levels, suggesting that in an intact heart, the repolarization of the action potential is sensitive to changes in intracellular NAD^+:NADH ratio.

To test whether the sensitivity of the action potential to intracellular levels of NAD(H) is due to Kvβ2 subunits, we recorded monophasic action potentials from isolated, perfused, $Kv\beta2^{-/-}$ hearts. Levels of NADH in $Kv\beta2^{-/-}$ hearts were similar to WT hearts (wt: 0.703 ± 0.222 pmoles/μg protein; $Kv\beta2^{-/-}$: 0.661 ± 0.096 pmoles/μg protein; P = 0.890, n = 4 each), and exhibited a significant increase upon application of 20 mM lactate (69 ± 21% increase

relative to control untreated hearts; n = 4 each; P = 0.037). Consistent with results suggesting that pyridine nucleotide sensitivity of Kv inactivation is lost in Kvβ2$^{-/-}$ myocytes, we found that the sensitivity of action potential duration to lactate was abolished in Kvβ2$^{-/-}$ hearts (Figure 7E, F; APD_{20}, P = 0.655; APD_{50}, P = 0.138; APD_{90}, P = 0.252). These results indicate that cardiac action potential duration is responsive to changes in intermediary metabolism that impact the redox status of pyridine nucleotides, and that this mode of membrane potential regulation is mediated by Kvβ2 subunits.

Discussion

The results of this study suggest that in murine hearts, Kvβ2 subunits play an important role in regulating the functional expression of voltage-gated K^+ channels, and in imparting metabolic sensitivity to these channels. A critical role of Kvβ2 in regulating the basal function of cardiac Kv channels is consistent with our observation that loss of Kvβ2 resulted in suppression of Kv current density (I_{to}, $I_{K,\ slow1}$, $I_{K,slow2}$), reduced sarcolemmal abundance of Kv proteins, and prolongation of the action potential. Moreover, our results provide direct evidence that the sensitivity of native cardiac Kv channel inactivation and repolarization to the redox state of pyridine nucleotides is imparted by Kvβ2 subunits.

Our data show that high intracellular values of the NAD(P)H:$NAD(P)^+$ ratio increase Kv channel inactivation, which may delay repolarization. The pyridine nucleotides are viewed primarily as electron carriers that shuttle electrons between different oxidation-reduction reactions of intermediary metabolism and as cofactors that support redox reactions in numerous metabolic processes. Yet, emerging evidence suggests that they play a more versatile role in cell physiology by participating in cell signaling, regulation of gene transcription, free radical production, and ion channel function [58]. Indeed, several ion channels and their regulatory subunits, such as Ca^{2+}-activated K^+ channel subunits *Slo1* and *Slo2*, Kir6.2, Nav1.5, CFTR, TPC2, TRPM2, RYR, and Kvβ contain nucleotide binding domains, which bind NAD(P)(H) with affinities within the range of their physiological intracellular concentrations [10]. The differential regulation of Kv activation and inactivation by oxidized (i.e., $NAD(P)^+$) and reduced (i.e., NAD(P)H) nucleotides, via the Kvβ subunits, has been proposed as a molecular mechanism by which cellular excitability is functionally coupled with cellular metabolism [59]. Considering that there are different Kv auxiliary subunits, each of which likely display unique responses to changes in cellular redox status, future studies are needed to address the complex issue of how different Kvβ proteins modulate Kv gating as a function of subunit stoichiometry, in the setting of fluctuating energetic demands. For instance, extensive evidence suggests that Kvβ2 subunits can be coexpressed in individual Kv auxiliary subunit complexes with Kvβ1, and that in addition to functional modulation of pore-forming proteins, Kvβ2 can also influence the inactivation function of Kvβ1 by competition for Kvα binding [60]. Thus, dynamic changes in the relative abundance of Kvβ2 and Kvβ1 in the heart may have profound effects on the kinetics and the voltage dependence of Kv currents, which may be important for fine tuning repolarization to the metabolic state of the heart as reflected by fluctuations in the redox state of pyridine nucleotides.

Changes in the redox state of pyridine nucleotides reflect the metabolic state of the heart and the levels of NADH, relative to NAD^+ rise with increased myocardial demand for oxygen [61]. We found that increasing the extracellular levels of lactate delayed action potential repolarization. Because perfusion with lactate was associated with an increase in NADH:NAD^+, we attribute the prolongation of action potential in the presence of lactate to changes in the redox state of pyridine nucleotides. Lactate could also affect the action potential; yet, this seems unlikely because neither the resting membrane potential nor dV/dt, both of which are sensitive to intracellular acidosis [62], were not affected by lactate. Nonetheless, it should be noted that changes in NADH:NAD^+ are known to modulate other currents that contribute to the cardiac action potential, such as I_{NCX} and I_{Na} [46, 63]. Therefore, it is possible that prolongation of the action potential, even if due to pyridine nucleotides, is mediated by changes in Kv-independent currents. However, this possibility seems unlikely as well, as we observed the direct regulation of Kv current by pyridine nucleotides in cardiac myocytes, and the effects of lactate in this study were absent in hearts lacking Kvβ2. Hence, the most plausible explanation of our findings is that lactate prolongs action potential duration by altering the redox state of intracellular nucleotides, which in turn modifies Kv currents. Although further work is required to elucidate the importance of Kvβ-dependent metabolic sensitivity in the context of arrhythmogenesis, it seems likely that this mode of regulation may serve to confer cardioprotection by promoting electrical refractoriness under conditions of reduced oxygen availability for the maintenance of energy homeostasis. Such a regulatory axis would be consistent with a critical function of Kvβ2 in preventing action potential over-shortening and arrhythmias upon metabolic activation of other types of K^+ channels (e.g., K_{ATP}) during ischemic or hypoxic conditions [64].

Beyond functional regulation of channel gating, substantial evidence supports the importance of Kv auxiliary proteins in supporting channel biosynthesis, intracellular trafficking, and functional expression of channels at the plasmalemma of excitable cells [11, 65]. Consistent with this view, we observed that the abundance of sarcolemmal Kv1 and Kv4 channels was reduced in myocytes of mice lacking Kvβ2 subunits, suggesting that in the heart, Kvβ2 plays an important role in localizing Kv channels to the membrane and in regulating the functional expression of I_{to} and $I_{K,slow}$. A similar role for Kvβ2 in promoting the surface expression of Kv1.5 in coronary arterial myocytes has been recently described by our group [35]. How Kvβ facilitates the targeting of Kv channels to the surface membrane remains to be fully clarified; however previous work suggests that the co-translational association of Kvβ2 protein with nascent Kvα polypeptide chains within the endoplasmic reticulum (ER) aids proper protein folding, and ER export of the complex [11]. The persistence of this α/β assembly may impart structural stabilization that likely contributes to a greater number of functional channels that are retained at the membrane. Indeed, products of all three Kvβ genes can promote plasmalemmal localization of Kv1.2 upon co-expression in COS-7 cells [66]. Thus, results of the current study are consistent with the concept that association of Kv1α subunits with Kvβ2 may indeed represent a chaperone mechanism inherent to these accessory subunits—regardless of the cell type in which they are expressed.

Molecular determinants of repolarizing K^+ currents in the heart comprise a complex composition of individual Kvα proteins, including members of the Kv1, Kv2, Kv4, Kv7, and Kv11 families. Adding to this molecular diversity, multiple ancillary subunits (e.g.,

minK, MiRP, KChIP, and Kvβ) are differentially associated with pore-forming α subunits. Indeed, the varied expression of this repertoire of Kv channel subunits in cardiac myocytes in a region-specific manner may reflect the profound physiological importance of precisely fine-tuned Kv currents for proper cardiac function, both spatially and temporally. The Kvβ proteins are known to associate with members of the Kv1 and Kv4 families, and previous work has shown that Kvβ1.1 and Kvβ1.2 subunits predominantly interact with Kv4.2 and Kv4.3 in adult mouse ventricles [25]. Our current results demonstrate interactions between Kvβ2 and Kv1.4 and Kv1.5 channels, which, unlike the Kv4 subunits, do not co-assemble as heteromeric channels in the heart, and generate distinct current profiles (i.e., $I_{to,s}$ and $I_{K,slow1}$, respectively) [67]. Our electrophysiological experiments suggest that Kvβ2 enhances Kv current density in the heart, which is at least partially attributed to enhanced Kv1 and Kv4 channel expression. Interestingly, a reduction in peak Kv current density upon ablation of Kvβ2 was also partially attributed to suppression of I_{to} density, which may reflect an influence of Kvβ2 on the function of $I_{to,f}$ due to the association of this auxiliary subunit with Kv4.2 and Kv4.3 channels [68]. The reasons for altered Kv current densities in Kvβ2$^{-/-}$ myocytes are likely multifaceted. In addition to the impact of Kvβ2 on surface expression of channels reported here, it is probable that this subunit also regulates gating of functional sarcolemmal Kv1 and Kv4 channels. Although the loss of Kvβ2 was not associated with significant differences in the inactivation rates of the examined I_{Kv} components, additional experiments are required to determine the specific contribution of this subunit on the voltage-dependencies and thresholds of activation of native Kv channels in the heart.

The observation that loss of Kvβ2 abolishes lactate-induced increases in APD suggests that this subunit is required for modulation of cardiomyocyte repolarization upon changes in the redox ration of pyridine nucleotides. However, in addition to Kvβ2, Kvβ1 also seems to be involved in such metabolic sensing as recent work has shown that the effect of lactate on APD are abolished in hearts isolated from Kvβ1.1$^{-/-}$ animals [39]. Thus, along with our present observations, these findings suggest that both Kvβ1 and Kvβ2 subunits function together to mediate metabolic sensitivity of Kv current densities and cardiac electrical activity, and therefore loss of either subunit may result in loss of metabolic sensitivity—even though the other subunit may be present. Such concomitant requirement of both auxiliary subunits for pyridine-nucleotide sensitivity of electrical signaling could be explained by the fundamental impact of the association between Kvα and Kvβ on channel activation properties shown in heterologous expression systems. Co-expression of either Kvβ1 and Kvβ2 subunits with Kv1α subunits shifts the voltage-dependence of channel activation by −10 to −15 mV [51, 52]. Thus, the absence of either Kvβ1 or Kvβ2 from native Kv channel complexes in cardiac myocytes may result in subpopulations of Kv channels with altered voltage-dependence and threshold of activation, which ultimately may lead to reduced contribution of Kv conductance toward repolarization. Consistent with this explanation, it has been found that basal APD is prolonged in the hearts of both Kvβ1.1$^{-/-}$ and Kvβ2$^{-/-}$ mice (see Figure 4 and [39]). Thus, even though Kvβ1 and Kvβ2 may disproportionately modulate distinct outward K^+ currents in the heart, the net effect of each subunit on channel gating may be a prerequisite for the modulation of repolarization in sync with changes in the redox state of pyridine nucleotides.

We found that loss of Kvβ2$^{-/-}$ altered heart morphology with modest changes in baseline cardiac function. It should be noted that in a previous study from our group, no significant changes in heart morphology were noted in male mice lacking Kvβ1.1 subunits [39]. However, Kvβ1.1 in murine hearts is bound to myosin heavy chain (MHCα) and ablation of Kvβ1.1 is associated with higher MHCα expression and hypertrophy in female mice [69]. In Kvβ2$^{-/-}$ mice, we noted significant reductions in cardiac myocyte size in the left ventricular endocardial and septal regions when compared with WT hearts (Figure 6). Although the underlying causes of these differences (e.g., hemodynamic, humoral) are unclear, our findings together with previous work suggests a unique role for Kvβ2 in regulating cardiac and skeletal muscle growth [9, 39, 44]. In addition to Kv channel subunits, Kvβ2 has been found to interact with multiple other proteins such as calmodulin, myosin, and E3 ubiqutin ligases [69–71]. Our prior work demonstrated that Kvβ2 regulates muscle growth via interactions with binding partners essential for muscle differentiation and growth such as NEDD4, which is known to stabilize membrane expression of several growth factor receptors (e.g., IGF-1R), which are essential for physiologic cardiac growth [44, 72, 73].

It has also been reported previously that the expression of K^+ channel subunits in the heart is increased during physiologic hypertrophic growth in response to exercise conditioning [74], which is thought to allow normalization of repolarizing current densities to increases in sarcolemmal surface area. However, it remains unclear whether Kv channels themselves participate in hypertrophic growth. In this regard, it is interesting to point out that due to the sensitivity of these channels to the redox state of pyridine nucleotides and their participation in regulating cell volume changes during cell growth [10], the metabolic regulation of these channels via Kvβ may be critical for coupling cell growth to cell metabolism. Clearly, additional research is warranted to address how Kv subunits impact cardiac hypertrophy under physiological (e.g., exercise) and pathological (e.g., hypertension) conditions. In view of our data showing that pyridine nucleotides regulate Kv currents via Kvβ subunits, investigations into the role of these subunits in regulating electrical signaling and cardiac function could yield important insights into the pathophysiology of ischemia-reperfusion injury, cardiomyopathy, and heart failure.

Despite robust evidence supporting the metabolic regulation of Kv channels by Kvβ, our study has several limitations. Although our data suggest that action potential duration is responsive to redox-mediated changes in K^+ currents, we did not directly test whether loss of Kvβ2 or changes in nucleotide redox result in alterations in I_{Na} or I_{Ca}. Thus, even though no changes in dV/dT_{max} or resting membrane potential were observed upon application of lactate, we cannot formally rule out modulation of other ionic currents that contribute to action potential duration. For instance, a trend towards reduced AP amplitude was noted in the presence of lactate, consistent with changes in I_{Na} [46]. In addition, we isolated myocytes for patch clamp experiments from the left ventricular, septal, and apical regions. It has been reported previously that significant differences exist, even within these regions, with respect to transmural gradients in K^+ channel subunit expression and action potential waveforms [75, 76]. Thus, the contribution of Kvβ2 to cardiac K^+ current may be contingent upon the specific myocyte population within a particular region of the heart. Nonetheless, our results demonstrating the lack of lactate-induced action potential prolongation in intact perfused hearts of Kvβ2$^{-/-}$ animals suggest that this protein contributes to the redox

sensitivity of cardiac repolarization of the heart as a whole, regardless of the specific distribution of Kv channels in myocyte subpopulations. Finally, we acknowledge the limitation inherent to studying cardiac electrophysiology in mice considering the substantial differences in ionic currents that exist between mice and larger mammals. Thus, our current findings should be considered in the context of discrepancies, particularly in repolarizing K^+ currents that contribute to key differences in the duration and overall shape of the action potential between mice and humans [77]. Thus, further investigations are needed to clarify the contribution of this subunit to the electrophysiology of larger mammals and human hearts.

In summary, we report here that cardiac Kvβ2 subunits contribute to the regulation of Kv current density and the modulation of action potential repolarization. These results suggest that the regulatory nature of Kvβ2 in the modulation of cardiac electrophysiology may be multifaceted, as this subunit appears to participate in the control of functional Kv expression (I_{to}, $I_{K,slow1}$, $I_{K,slow2}$), the modulation of channel inactivation properties, and in imparting pyridine nucleotide sensitivity to Kv channels.

Supplementary Material

Refer to Web version on PubMed Central for supplementary material.

Acknowledgements

We thank Dr. Ganapathy Jagatheesan and Mr. Zachary Wohl for technical assistance. This work was supported in part by grants from the National Institutes of Health (HL142710, HL102171, HL131647, HL078825, and GM103492), American Heart Association (16SDG27260070), and the University of Louisville, School of Medicine.

REFERENCES

[1]. Nerbonne JM, Molecular Basis of Functional Myocardial Potassium Channel Diversity, Card Electrophysiol Clin 8(2) (2016) 257–73. [PubMed: 27261820]

[2]. Grant AO, Cardiac ion channels, Circ Arrhythm Electrophysiol 2(2) (2009) 185–94. [PubMed: 19808464]

[3]. Olson TM, Alekseev AE, Liu XK, Park S, Zingman LV, Bienengraeber M, Sattiraju S, Ballew JD, Jahangir A, Terzic A, Kv1.5 channelopathy due to KCNA5 loss-of-function mutation causes human atrial fibrillation, Hum Mol Genet 15(14) (2006) 2185–91. [PubMed: 16772329]

[4]. Christophersen IE, Olesen MS, Liang B, Andersen MN, Larsen AP, Nielsen JB, Haunso S, Olesen SP, Tveit A, Svendsen JH, Schmitt N, Genetic variation in KCNA5: impact on the atrial-specific potassium current IKur in patients with lone atrial fibrillation, Eur Heart J 34(20) (2013) 1517–25. [PubMed: 23264583]

[5]. London B, Jeron A, Zhou J, Buckett P, Han X, Mitchell GF, Koren G, Long QT and ventricular arrhythmias in transgenic mice expressing the N terminus and first transmembrane segment of a voltage-gated potassium channel, Proceedings of the National Academy of Sciences of the United States of America 95(6) (1998) 2926–31. [PubMed: 9501192]

[6]. Barry DM, Xu H, Schuessler RB, Nerbonne JM, Functional knockout of the transient outward current, long-QT syndrome, and cardiac remodeling in mice expressing a dominant-negative Kv4 alpha subunit, Circulation research 83(5) (1998) 560–7. [PubMed: 9734479]

[7]. Guo W, Li H, London B, Nerbonne JM, Functional consequences of elimination of i(to,f) and i(to,s): early afterdepolarizations, atrioventricular block, and ventricular arrhythmias in mice

lacking Kv1.4 and expressing a dominant-negative Kv4 alpha subunit, Circulation research 87(1) (2000) 73–9. [PubMed: 10884375]

[8]. Pongs O, Schwarz JR, Ancillary subunits associated with voltage-dependent K+ channels, Physiol Rev 90(2) (2010) 755–96. [PubMed: 20393197]

[9]. McCormack K, Connor JX, Zhou L, Ho LL, Ganetzky B, Chiu SY, Messing A, Genetic analysis of the mammalian K+ channel beta subunit Kvbeta 2 (Kcnab2), The Journal of biological chemistry 277(15) (2002) 13219–28. [PubMed: 11825900]

[10]. Kilfoil PJ, Tipparaju SM, Barski OA, Bhatnagar A, Regulation of ion channels by pyridine nucleotides, Circulation research 112(4) (2013) 721–41. [PubMed: 23410881]

[11]. Shi G, Nakahira K, Hammond S, Rhodes KJ, Schechter LE, Trimmer JS, Beta subunits promote K+ channel surface expression through effects early in biosynthesis, Neuron 16(4) (1996) 843–52. [PubMed: 8608002]

[12]. Tiffany AM, Manganas LN, Kim E, Hsueh YP, Sheng M, Trimmer JS, PSD-95 and SAP97 exhibit distinct mechanisms for regulating K(+) channel surface expression and clustering, The Journal of cell biology 148(1) (2000) 147–58. [PubMed: 10629225]

[13]. Yang EK, Alvira MR, Levitan ES, Takimoto K, Kvbeta subunits increase expression of Kv4.3 channels by interacting with their C termini, The Journal of biological chemistry 276(7) (2001) 4839–44. [PubMed: 11087728]

[14]. Vacher H, Trimmer JS, Trafficking mechanisms underlying neuronal voltage-gated ion channel localization at the axon initial segment, Epilepsia 53 Suppl 9 (2012) 21–31. [PubMed: 23216576]

[15]. Gu C, Zhou W, Puthenveedu MA, Xu M, Jan YN, Jan LY, The microtubule plus-end tracking protein EB1 is required for Kv1 voltage-gated K+ channel axonal targeting, Neuron 52(5) (2006) 803–16. [PubMed: 17145502]

[16]. Accili EA, Kiehn J, Yang Q, Wang Z, Brown AM, Wible BA, Separable Kvbeta subunit domains alter expression and gating of potassium channels, The Journal of biological chemistry 272(41) (1997) 25824–31. [PubMed: 9325312]

[17]. Rettig J, Heinemann SH, Wunder F, Lorra C, Parcej DN, Dolly JO, Pongs O, Inactivation properties of voltage-gated K+ channels altered by presence of beta-subunit, Nature 369(6478) (1994) 289–94. [PubMed: 8183366]

[18]. McIntosh P, Southan AP, Akhtar S, Sidera C, Ushkaryov Y, Dolly JO, Robertson B, Modification of rat brain Kv1.4 channel gating by association with accessory Kvbeta1.1 and beta2.1 subunits, Pflugers Arch 435(1) (1997) 43–54. [PubMed: 9359902]

[19]. Leicher T, Bahring R, Isbrandt D, Pongs O, Coexpression of the KCNA3B gene product with Kv1.5 leads to a novel A-type potassium channel, The Journal of biological chemistry 273(52) (1998) 35095–101. [PubMed: 9857044]

[20]. Liu SQ, Jin H, Zacarias A, Srivastava S, Bhatnagar A, Binding of pyridine nucleotide coenzymes to the beta-subunit of the voltage-sensitive K+ channel, The Journal of biological chemistry 276(15) (2001) 11812–20. [PubMed: 11278398]

[21]. Tipparaju SM, Liu SQ, Barski OA, Bhatnagar A, NADPH binding to beta-subunit regulates inactivation of voltage-gated K(+) channels, Biochemical and biophysical research communications 359(2) (2007) 269–76. [PubMed: 17540341]

[22]. Weng J, Cao Y, Moss N, Zhou M, Modulation of voltage-dependent Shaker family potassium channels by an aldo-keto reductase, The Journal of biological chemistry 281(22) (2006) 15194–200. [PubMed: 16569641]

[23]. Tipparaju SM, Barski OA, Srivastava S, Bhatnagar A, Catalytic mechanism and substrate specificity of the beta-subunit of the voltage-gated potassium channel, Biochemistry 47(34) (2008) 8840–54. [PubMed: 18672894]

[24]. Alka K, Ryan BJ, Dolly JO, Henehan GT, Substrate profiling and aldehyde dismutase activity of the Kvbeta2 subunit of the mammalian Kv1 potassium channel, Int J Biochem Cell Biol 42(12) (2010) 2012–8. [PubMed: 20833259]

[25]. Aimond F, Kwak SP, Rhodes KJ, Nerbonne JM, Accessory Kvbeta1 subunits differentially modulate the functional expression of voltage-gated K+ channels in mouse ventricular myocytes, Circulation research 96(4) (2005) 451–8. [PubMed: 15662035]

[26]. Portero V, Le Scouarnec S, Es-Salah-Lamoureux Z, Burel S, Gourraud JB, Bonnaud S, Lindenbaum P, Simonet F, Violleau J, Baron E, Moreau E, Scott C, Chatel S, Loussouarn G, O'Hara T, Mabo P, Dina C, Le Marec H, Schott JJ, Probst V, Baro I, Marionneau C, Charpentier F, Redon R, Dysfunction of the Voltage-Gated K+ Channel beta2 Subunit in a Familial Case of Brugada Syndrome, J Am Heart Assoc 5(6) (2016).

[27]. Perkowski JJ, Murphy GG, Deletion of the mouse homolog of KCNAB2, a gene linked to monosomy 1p36, results in associative memory impairments and amygdala hyperexcitability, The Journal of neuroscience : the official journal of the Society for Neuroscience 31(1) (2011) 46–54. [PubMed: 21209188]

[28]. Conklin DJ, Guo Y, Jagatheesan G, Kilfoil PJ, Haberzettl P, Hill BG, Baba SP, Guo L, Wetzelberger K, Obal D, Rokosh DG, Prough RA, Prabhu SD, Velayutham M, Zweier JL, Hoetker JD, Riggs DW, Srivastava S, Bolli R, Bhatnagar A, Genetic Deficiency of Glutathione S-Transferase P Increases Myocardial Sensitivity to Ischemia-Reperfusion Injury, Circulation research 117(5) (2015) 437–49. [PubMed: 26169370]

[29]. Greer JJ, Kakkar AK, Elrod JW, Watson LJ, Jones SP, Lefer DJ, Low-dose simvastatin improves survival and ventricular function via eNOS in congestive heart failure, American journal of physiology. Heart and circulatory physiology 291(6) (2006) H2743–51. [PubMed: 16844920]

[30]. Dassanayaka S, Brainard RE, Watson LJ, Long BW, Brittian KR, DeMartino AM, Aird AL, Gumpert AM, Audam TN, Kilfoil PJ, Muthusamy S, Hamid T, Prabhu SD, Jones SP, Cardiomyocyte Ogt limits ventricular dysfunction in mice following pressure overload without affecting hypertrophy, Basic Res Cardiol 112(3) (2017) 23. [PubMed: 28299467]

[31]. Wang J, Wang Q, Watson LJ, Jones SP, Epstein PN, Cardiac overexpression of 8-oxoguanine DNA glycosylase 1 protects mitochondrial DNA and reduces cardiac fibrosis following transaortic constriction, American journal of physiology. Heart and circulatory physiology 301(5) (2011) H2073–80. [PubMed: 21873502]

[32]. Chapalamadugu KC, Panguluri SK, Bennett ES, Kolliputi N, Tipparaju SM, High level of oxygen treatment causes cardiotoxicity with arrhythmias and redox modulation, Toxicol Appl Pharmacol 282(1) (2015) 100–7. [PubMed: 25447406]

[33]. Gu C, Jan YN, Jan LY, A conserved domain in axonal targeting of Kv1 (Shaker) voltage-gated potassium channels, Science 301(5633) (2003) 646–9. [PubMed: 12893943]

[34]. Goodwill AG, Noblet JN, Sassoon D, Fu L, Kassab GS, Schepers L, Herring BP, Rottgen TS, Tune JD, Dick GM, Critical contribution of KV1 channels to the regulation of coronary blood flow, Basic Res Cardiol 111(5) (2016) 56. [PubMed: 27496159]

[35]. Nystoriak MA, Zhang D, Jagatheesan G, Bhatnagar A, Heteromeric complexes of aldo-keto reductase auxiliary KVbeta subunits (AKR6A) regulate sarcolemmal localization of KV1.5 in coronary arterial myocytes, Chem Biol Interact (2017).

[36]. Nystoriak MA, Nieves-Cintron M, Patriarchi T, Buonarati OR, Prada MP, Morotti S, Grandi E, Fernandes JD, Forbush K, Hofmann F, Sasse KC, Scott JD, Ward SM, Hell JW, Navedo MF, Ser1928 phosphorylation by PKA stimulates the L-type Ca2+ channel CaV1.2 and vasoconstriction during acute hyperglycemia and diabetes, Sci Signal 10(463) (2017).

[37]. Takimoto K, Levitan ES, Glucocorticoid induction of Kv1.5 K+ channel gene expression in ventricle of rat heart, Circulation research 75(6) (1994) 1006–13. [PubMed: 7955140]

[38]. Nguyen LH, Anderson AE, mTOR-dependent alterations of Kv1.1 subunit expression in the neuronal subset-specific Pten knockout mouse model of cortical dysplasia with epilepsy, Sci Rep 8(1) (2018) 3568. [PubMed: 29476105]

[39]. Tur J, Chapalamadugu KC, Katnik C, Cuevas J, Bhatnagar A, Tipparaju SM, Kvbeta1.1 (AKR6A8) senses pyridine nucleotide changes in the mouse heart and modulates cardiac electrical activity, American journal of physiology. Heart and circulatory physiology 312(3) (2017) H571–H583. [PubMed: 27986658]

[40]. Huang H, Amin V, Gurin M, Wan E, Thorp E, Homma S, Morrow JP, Diet-induced obesity causes long QT and reduces transcription of voltage-gated potassium channels, Journal of molecular and cellular cardiology 59 (2013) 151–8. [PubMed: 23517696]

[41]. Khandekar A, Springer S, Wang W, Hicks S, Weinheimer C, Diaz-Trelles R, Nerbonne JM, Rentschler S, Notch-Mediated Epigenetic Regulation of Voltage-Gated Potassium Currents, Circulation research 119(12) (2016) 1324–1338. [PubMed: 27697822]

[42]. Cheng L, Al-Owais M, Covarrubias ML, Koch WJ, Manning DR, Peers C, Riobo-Del Galdo NA, Coupling of Smoothened to inhibitory G proteins reduces voltage-gated K(+) currents in cardiomyocytes and prolongs cardiac action potential duration, The Journal of biological chemistry 293(28) (2018) 11022–11032. [PubMed: 29802197]

[43]. El Gebeily G, El Khoury N, Mathieu S, Brouillette J, Fiset C, Estrogen regulation of the transient outward K(+) current involves estrogen receptor alpha in mouse heart, Journal of molecular and cellular cardiology 86 (2015) 85–94. [PubMed: 26205295]

[44]. Chapalamadugu KC, Tur J, Badole SL, Kukreja RC, Brotto M, Tipparaju SM, Physiological role of Kvbeta2 (AKR6) in murine skeletal muscle growth and regulation, Acta Physiol (Oxf) 224(2) (2018) e13083. [PubMed: 29704886]

[45]. Panama BK, Korogyi AS, Aschar-Sobbi R, Oh Y, Gray CB, Gang H, Brown JH, Kirshenbaum LA, Backx PH, Reductions in the Cardiac Transient Outward K+ Current Ito Caused by Chronic beta-Adrenergic Receptor Stimulation Are Partly Rescued by Inhibition of Nuclear Factor kappaB, The Journal of biological chemistry 291(8) (2016) 4156–65. [PubMed: 26742842]

[46]. Liu M, Sanyal S, Gao G, Gurung IS, Zhu X, Gaconnet G, Kerchner LJ, Shang LL, Huang CL, Grace A, London B, Dudley SC Jr., Cardiac Na+ current regulation by pyridine nucleotides, Circulation research 105(8) (2009) 737–45. [PubMed: 19745168]

[47]. Bondarenko VE, Szigeti GP, Bett GC, Kim SJ, Rasmusson RL, Computer model of action potential of mouse ventricular myocytes, American journal of physiology. Heart and circulatory physiology 287(3) (2004) H1378–403. [PubMed: 15142845]

[48]. Gaborit N, Varro A, Le Bouter S, Szuts V, Escande D, Nattel S, Demolombe S, Genderrelated differences in ion-channel and transporter subunit expression in non-diseased human hearts, Journal of molecular and cellular cardiology 49(4) (2010) 639–46. [PubMed: 20600101]

[49]. Abriel H, Rougier JS, Jalife J, Ion channel macromolecular complexes in cardiomyocytes: roles in sudden cardiac death, Circulation research 116(12) (2015) 1971–88. [PubMed: 26044251]

[50]. Liu J, Kim KH, Morales MJ, Heximer SP, Hui CC, Backx PH, Kv4.3-Encoded Fast Transient Outward Current Is Presented in Kv4.2 Knockout Mouse Cardiomyocytes, PloS one 10(7) (2015) e0133274. [PubMed: 26196737]

[51]. Tipparaju SM, Saxena N, Liu SQ, Kumar R, Bhatnagar A, Differential regulation of voltage-gated K+ channels by oxidized and reduced pyridine nucleotide coenzymes, American journal of physiology. Cell physiology 288(2) (2005) C366–76. [PubMed: 15469953]

[52]. Tipparaju SM, Li XP, Kilfoil PJ, Xue B, Uversky VN, Bhatnagar A, Barski OA, Interactions between the C-terminus of Kv1.5 and Kvbeta regulate pyridine nucleotidedependent changes in channel gating, Pflugers Arch 463(6) (2012) 799–818. [PubMed: 22426702]

[53]. Glock GE, McLean P, Levels of oxidized and reduced diphosphopyridine nucleotide and triphosphopyridine nucleotide in animal tissues, Biochem J 61(3) (1955) 388–90. [PubMed: 13269372]

[54]. Bessho M, Tajima T, Hori S, Satoh T, Fukuda K, Kyotani S, Ohnishi Y, Nakamura Y, NAD and NADH values in rapidly sampled dog heart tissues by two different extraction methods, Anal Biochem 182(2) (1989) 304–8. [PubMed: 2610348]

[55]. Lane M, Gardner DK, Lactate regulates pyruvate uptake and metabolism in the preimplantation mouse embryo, Biol Reprod 62(1) (2000) 16–22. [PubMed: 10611062]

[56]. Hung YP, Albeck JG, Tantama M, Yellen G, Imaging cytosolic NADH-NAD(+) redox state with a genetically encoded fluorescent biosensor, Cell Metab 14(4) (2011) 545–54. [PubMed: 21982714]

[57]. Sun F, Dai C, Xie J, Hu X, Biochemical issues in estimation of cytosolic free NAD/NADH ratio, PloS one 7(5) (2012) e34525. [PubMed: 22570687]

[58]. Pollak N, Dolle C, Ziegler M, The power to reduce: pyridine nucleotides--small molecules with a multitude of functions, Biochem J 402(2) (2007) 205–18. [PubMed: 17295611]

[59]. McCormack T, McCormack K, Shaker K+ channel beta subunits belong to an NAD(P)H-dependent oxidoreductase superfamily, Cell 79(7) (1994) 1133–5. [PubMed: 8001150]

[60]. Xu J, Li M, Kvbeta2 inhibits the Kvbeta1-mediated inactivation of K+ channels in transfected mammalian cells, The Journal of biological chemistry 272(18) (1997) 11728–35. [PubMed: 9115226]

[61]. Wengrowski AM, Kuzmiak-Glancy S, Jaimes R 3rd, Kay MW, NADH changes during hypoxia, ischemia, and increased work differ between isolated heart preparations, American journal of physiology. Heart and circulatory physiology 306(4) (2014) H529–37. [PubMed: 24337462]

[62]. Gasser RN, Vaughan-Jones RD, Mechanism of potassium efflux and action potential shortening during ischaemia in isolated mammalian cardiac muscle, The Journal of physiology 431 (1990) 713–41. [PubMed: 2129231]

[63]. Liu T, O'Rourke B, Regulation of the Na+/Ca2+ exchanger by pyridine nucleotide redox potential in ventricular myocytes, The Journal of biological chemistry 288(44) (2013) 31984–92. [PubMed: 24045952]

[64]. Suzuki M, Sasaki N, Miki T, Sakamoto N, Ohmoto-Sekine Y, Tamagawa M, Seino S, Marban E, Nakaya H, Role of sarcolemmal K(ATP) channels in cardioprotection against ischemia/reperfusion injury in mice, The Journal of clinical investigation 109(4) (2002) 509–16. [PubMed: 11854323]

[65]. Manganas LN, Trimmer JS, Subunit composition determines Kv1 potassium channel surface expression, The Journal of biological chemistry 275(38) (2000) 29685–93. [PubMed: 10896669]

[66]. Campomanes CR, Carroll KI, Manganas LN, Hershberger ME, Gong B, Antonucci DE, Rhodes KJ, Trimmer JS, Kv beta subunit oxidoreductase activity and Kv1 potassium channel trafficking, The Journal of biological chemistry 277(10) (2002) 8298–305. [PubMed: 11748234]

[67]. London B, Guo W, Pan X, Lee JS, Shusterman V, Rocco CJ, Logothetis DA, Nerbonne JM, Hill JA, Targeted replacement of KV1.5 in the mouse leads to loss of the 4-aminopyridine-sensitive component of I(K,slow) and resistance to drug-induced qt prolongation, Circulation research 88(9) (2001) 940–6. [PubMed: 11349004]

[68]. Guo W, Jung WE, Marionneau C, Aimond F, Xu H, Yamada KA, Schwarz TL, Demolombe S, Nerbonne JM, Targeted deletion of Kv4.2 eliminates I(to,f) and results in electrical and molecular remodeling, with no evidence of ventricular hypertrophy or myocardial dysfunction, Circulation research 97(12) (2005) 1342–50. [PubMed: 16293790]

[69]. Tur J, Chapalamadugu KC, Padawer T, Badole SL, Kilfoil, PJ 2nd, Bhatnagar A, Tipparaju SM, Deletion of Kvbeta1.1 subunit leads to electrical and haemodynamic changes causing cardiac hypertrophy in female murine hearts, Exp Physiol 101(4) (2016) 494–508. [PubMed: 27038296]

[70]. Swain SM, Sahoo N, Dennhardt S, Schonherr R, Heinemann SH, Ca(2+)/calmodulin regulates Kvbeta1.1-mediated inactivation of voltage-gated K(+) channels, Sci Rep 5 (2015) 15509. [PubMed: 26487174]

[71]. Persaud A, Alberts P, Amsen EM, Xiong X, Wasmuth J, Saadon Z, Fladd C, Parkinson J, Rotin D, Comparison of substrate specificity of the ubiquitin ligases Nedd4 and Nedd4–2 using proteome arrays, Mol Syst Biol 5 (2009) 333. [PubMed: 19953087]

[72]. Cao XR, Lill NL, Boase N, Shi PP, Croucher DR, Shan H, Qu J, Sweezer EM, Place T, Kirby PA, Daly RJ, Kumar S, Yang B, Nedd4 controls animal growth by regulating IGF-1 signaling, Sci Signal 1(38) (2008) ra5. [PubMed: 18812566]

[73]. McMullen JR, Shioi T, Huang WY, Zhang L, Tarnavski O, Bisping E, Schinke M, Kong S, Sherwood MC, Brown J, Riggi L, Kang PM, Izumo S, The insulin-like growth factor 1 receptor induces physiological heart growth via the phosphoinositide 3-kinase(p110alpha) pathway, The Journal of biological chemistry 279(6) (2004) 4782–93. [PubMed: 14597618]

[74]. Yang KC, Foeger NC, Marionneau C, Jay PY, McMullen JR, Nerbonne JM, Homeostatic regulation of electrical excitability in physiological cardiac hypertrophy, The Journal of physiology 588(Pt 24) (2010) 5015–32. [PubMed: 20974681]

[75]. Clark RB, Bouchard RA, Salinas-Stefanon E, Sanchez-Chapula J, Giles WR, Heterogeneity of action potential waveforms and potassium currents in rat ventricle, Cardiovascular research 27(10) (1993) 1795–9. [PubMed: 8275526]

[76]. Rossow CF, Dilly KW, Santana LF, Differential calcineurin/NFATc3 activity contributes to the Ito transmural gradient in the mouse heart, Circulation research 98(10) (2006) 1306–13. [PubMed: 16614306]

[77]. Nerbonne JM, Studying cardiac arrhythmias in the mouse--a reasonable model for probing mechanisms?, Trends Cardiovasc Med 14(3) (2004) 83–93. [PubMed: 15121155]

Highlights

- Kv auxiliary Kvβ2 subunits interact with Kv1 and Kv4 channels in the murine heart.
- Ablation of Kvβ2 leads to suppression of Ito, IK,slow1 and IK,slow2, and prolongs action potential duration.
- Dialysis of pyridine nucleotide ratios simulating hypoxic conditions enhance Kv inactivation in wild type, but not $Kv\beta2^{-/-}$ cardiac myocytes.
- Lactate increases NADH:NAD_+ ratio and prolongs action potential duration in wild type, but not $Kv\beta2^{-/-}$ hearts.

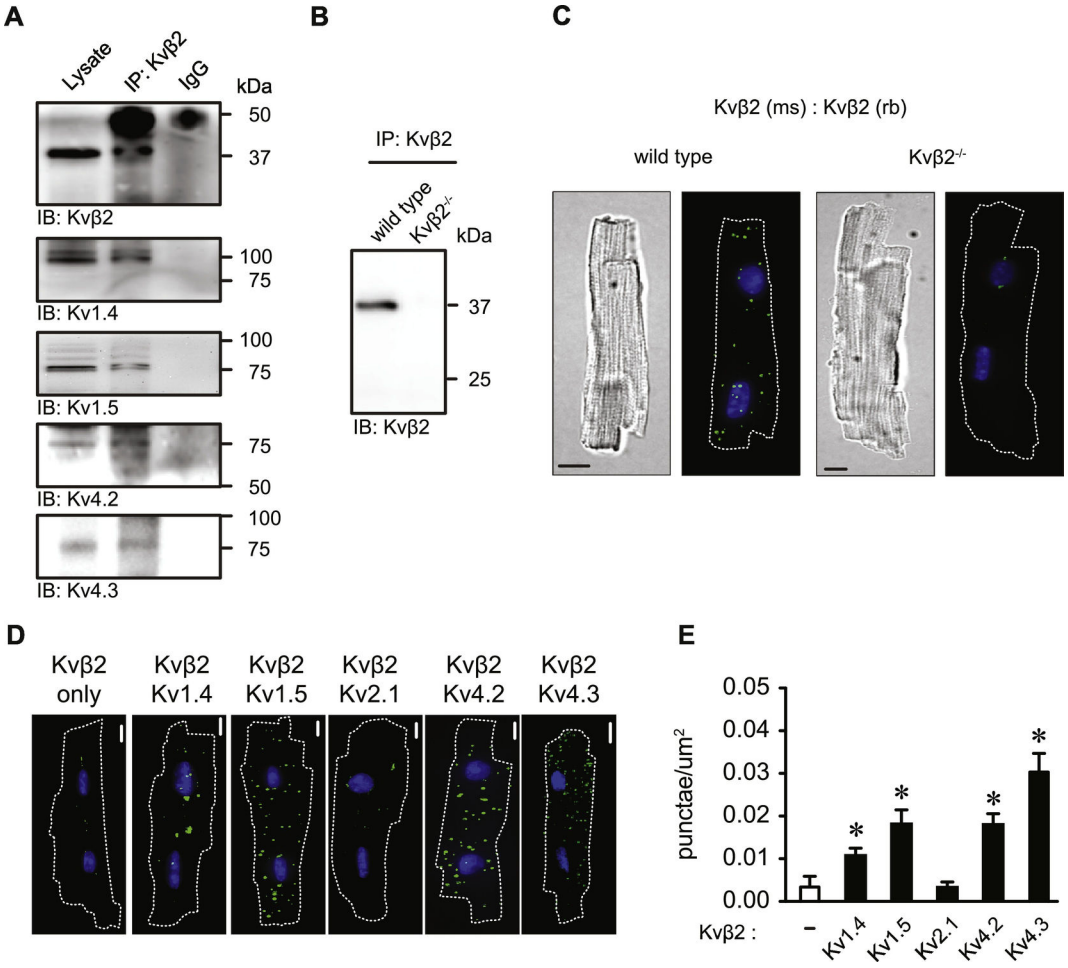

Figure 1: Myocardial Kvβ2 associates with Kv1 and Kv4 proteins.

(**A**) Representative blot images showing immunoreactive bands for Kv1.4, Kv1.5, Kv4.2, Kv4.3 and Kvβ2 in whole heart lysates and Kvβ2 immunoprecipitates. Absence of immunoreactive bands at expected molecular weights for each protein is also shown for mouse IgG immunoprecipitates as a negative control. Representative of 3 independent experiments. (**B**) Representative blot image showing immunoreactivity for Kvβ2 (predicted molecular weight, ~37 kDa) in Kvβ2 immunoprecipitates from heart lysates of wild type and Kvβ2$^{-/-}$ animals. (**C**) Differential interference contrast (DIC) and proximity ligation assay (PLA)-associated fluorescence images of isolated adult ventricular myocytes from wild type and Kvβ2$^{-/-}$ animals after PLA targeting of Kvβ2 complexes using mouse and rabbit-derived anti-Kvβ2 primary antibodies. PLA images are shown as flattened 2D maximum intensity z-projections from z-series captured for each cell. (**D**) PLA images of isolated ventricular myocytes treated with anti-Kvβ2 only, or anti-Kvβ2 with anti-Kv1.4, anti-Kv1.5, anti-Kv2.1 anti-Kv4.2, anti-Kv4.3. (**E**) Summary of fluorescent PLA-associated punctae, normalized to cell footprint area, for cells treated with anti-Kvβ2 only, or anti-Kvβ2 with anti-Kv1.4, anti-Kv1.5, anti-Kv2.1, anti-Kv4.2 and anti-Kv4.3 primary antibodies (n = 6–10). *P<0.05 vs. anti-Kvβ2 only (−) group.

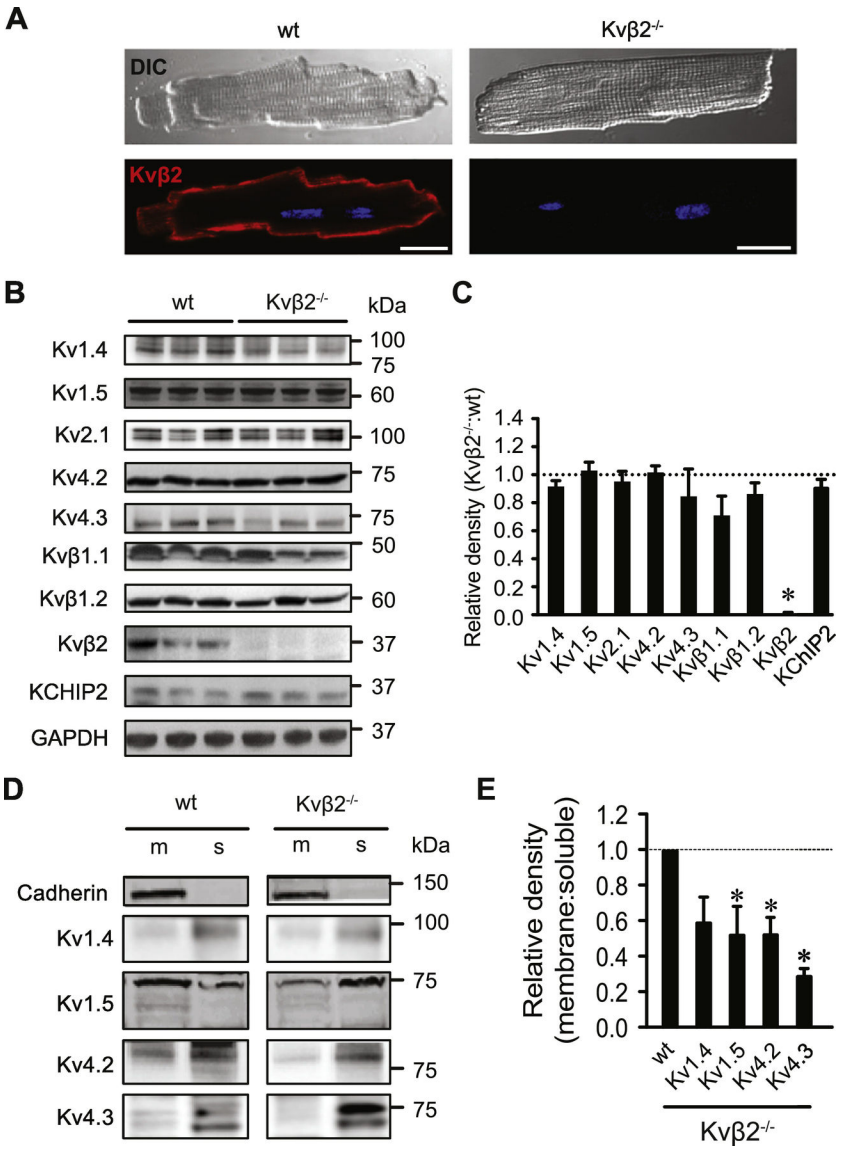

Figure 2: Kvβ2 promotes Kv1 and Kv4 surface expression in cardiac myocytes.

(**A**) Differential interference contrast (DIC) and confocal images showing Kvβ2-associated fluorescence (red) in isolated cardiac myocytes from wild type (wt) and Kvβ2$^{-/-}$ animals. Nuclei (dapi) are shown in blue. (**B**) Western blots showing immunoreactive bands for Kv pore-forming and auxiliary subunits at respective predicted molecular weights as indicated in heart lysates from wt (n = 3) and Kvβ2$^{-/-}$ (n = 3) animals. As a representative loading control, immunoreactive bands for GAPDH are shown for each lane of Kv1.5 blot. (**C**) Summarized densitometric data for Kv1.4, Kv1.5, Kv2.1, Kv4.2, Kv4.3, Kvβ1.1, Kvβ1.2, Kvβ2, and KChIP2 proteins in heart lysates of wt animals. Data are normalized to GAPDH (run for each blot) and expressed relative to wt controls. *P<0.05. (**D, E**) Representative Western blot images (D) showing immunoreactive bands for Kv1.4, Kv1.5, Kv4.2, and Kv4.3 and cadherin in cardiac myocyte membrane (m) and soluble (s) fractions and summary densitometric data (E) demonstrating membrane abundance of Kv1.4, Kv1.5,

Kv4.2, and Kv4.3, expressed as the membrane:soluble band densities in hearts from $K\nu\beta2^{-/-}$ mice relative to that in hearts from wild type mice. (n = 3–5 hearts) *P<0.05.

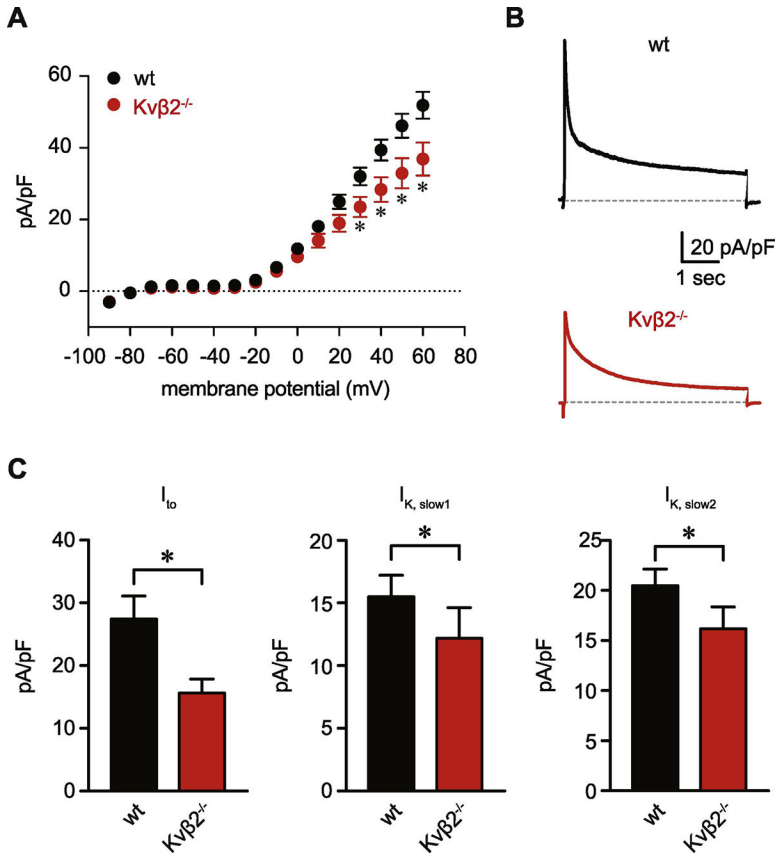

Figure 3: Suppressed Kv current density in cardiac myocytes from Kvβ2$^{-/-}$ mice.

(**A**) Summary current-voltage relationship obtained from cardiac myocytes from wild type and Kvβ2$^{-/-}$ animals. **(B)** Representative outward K^+ current recordings normalized to cell capacitance (pA/pF) in response to a pulse depolarization to +50 mV from a holding potential of −80 mV in ventricular myocytes from wt and Kvβ2$^{-/-}$ animals. **(C)** Summarized current density magnitudes for I_{to}, $I_{K,slow1}$, and $I_{K,slow2}$ components, obtained from tri-exponential fitting of +50 mV-elicited current recordings, as shown in panel A, for wt and Kvβ2$^{-/-}$ myocytes (n = 15–19 cells from 4–6 mice). *P<0.05.

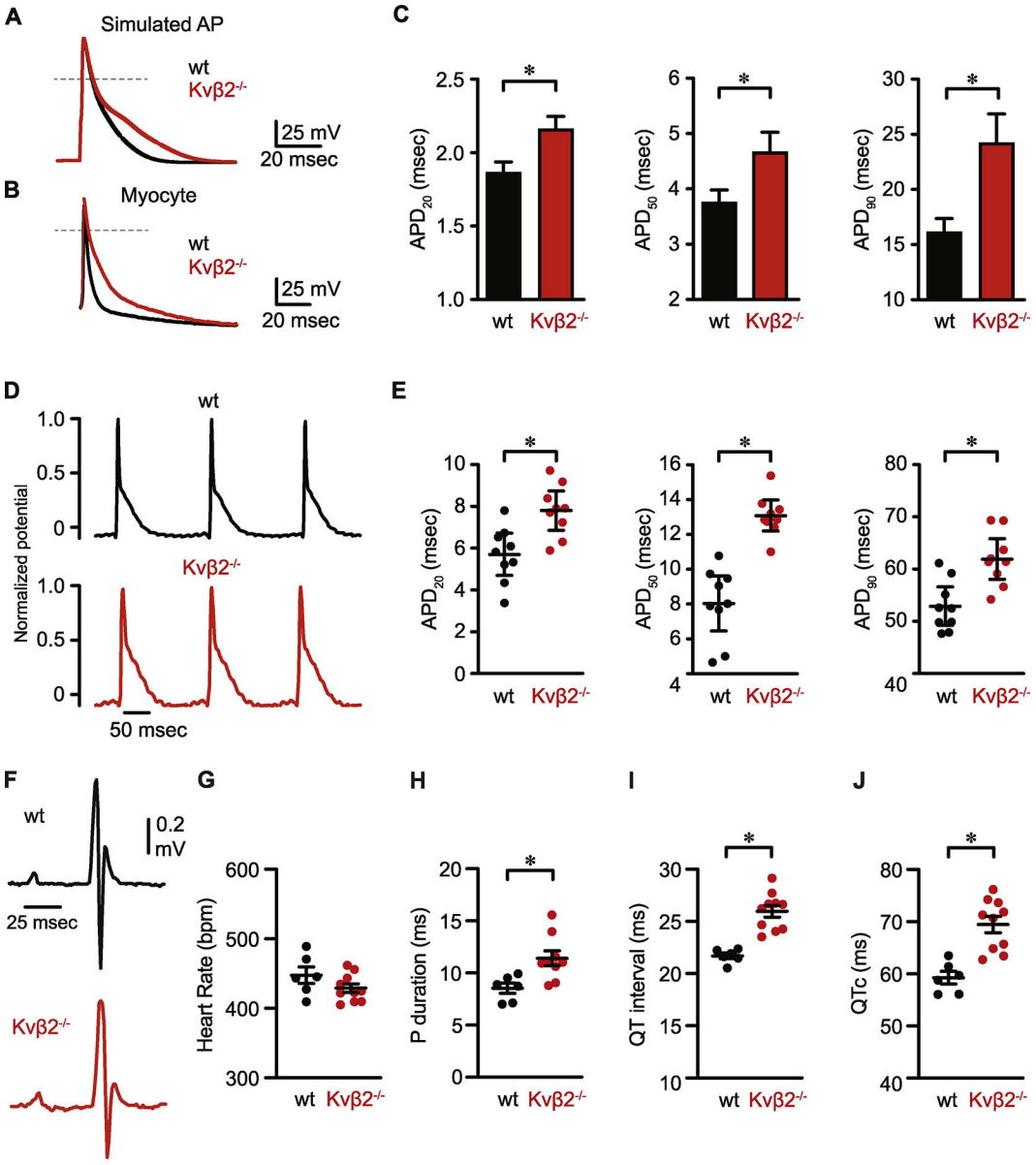

Figure 4: Delayed action potential repolarization in cardiac myocytes from Kvβ2$^{-/-}$ mice.

(**A**) Simulations showing normal mouse action potential (wt) and after scaling model parameters to reflect the reduction in current density components observed in Kvβ2$^{-/-}$ ventricular myocytes. (**B**) Representative overlaid action potentials recorded (conventional whole cell; current clamp) from wt and Kvβ2$^{-/-}$ ventricular myocytes. (**C**) Summary of action potential durations at 20%, 50%, and 90% repolarization in ventricular myocytes from wt (n = 17 cells from 5 mice) and Kvβ2$^{-/-}$ (n = 15 cells from 6 mice) animals. (**D**) Representative monophasic action potential recordings normalized to peak potential obtained from the left ventricular epicardial surface of hearts from wild type and Kvβ2$^{-/-}$ animals. (**E**) Scatter plots showing MAP durations at 20%, 50%, and 90% repolarization in hearts from wt and Kvβ2$^{-/-}$ (n = 9 hearts each) animals. (**F-J**) Representative ECG

waveforms and summarized heart rate, P duration, QT interval and QTc in wild type (n = 6) and Kvβ2$^{-/-}$ (n = 10) mice *P<0.05.

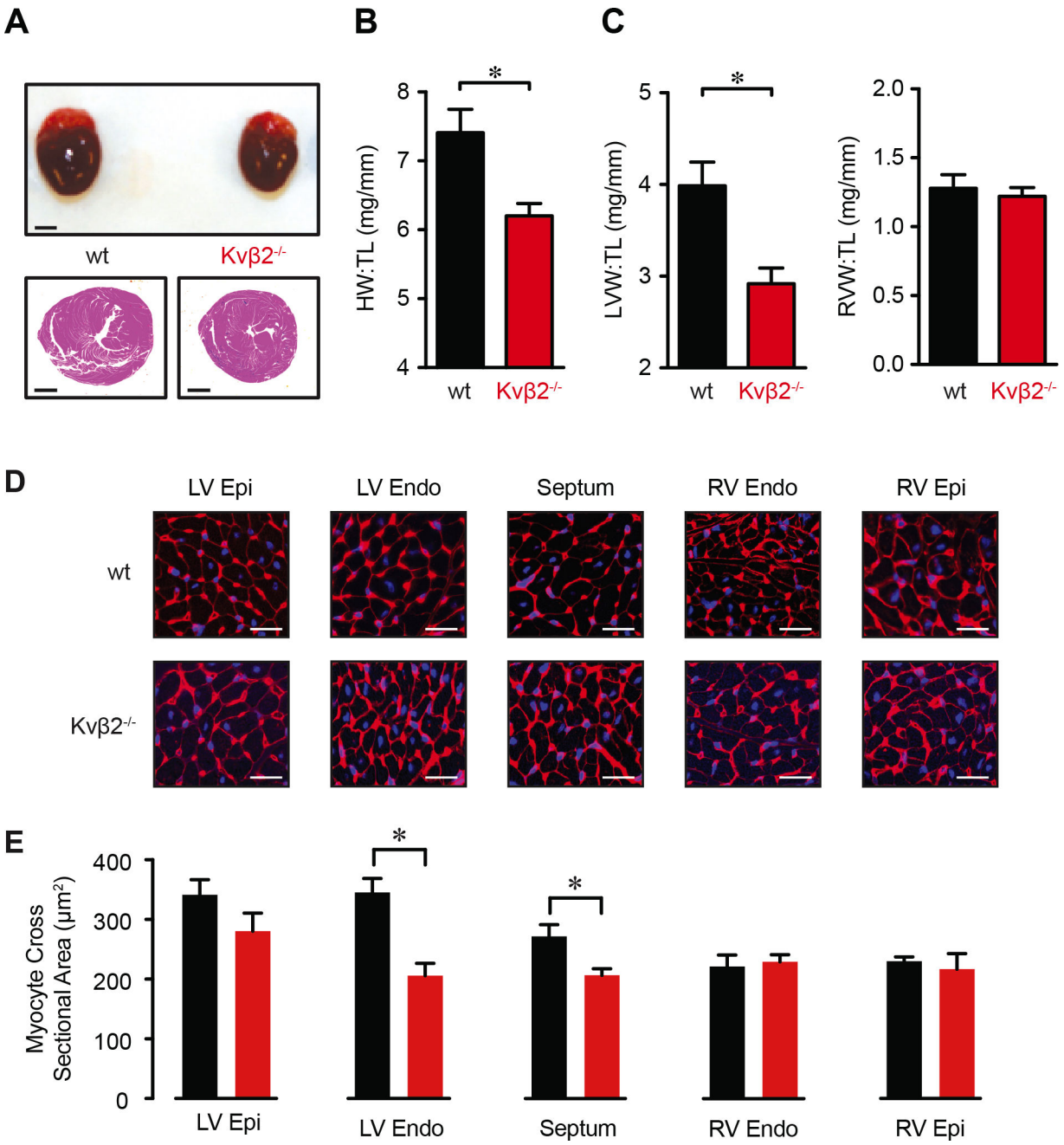

Figure 5: Loss of Kvβ2 alters heart morphology.

(**A**) Images showing whole hearts (*top*; scale bar = 2 mm) and hematoxylin and eosin stained transverse heart sections (*bottom*; scale bar = 1 mm). (**B, C**) Total heart weight (HW; **B**) and left and right ventricular weight (LVW, RVW; **C**) normalized to tibia length (TL) for hearts from wt (n = 12) and Kvβ2$^{-/-}$ (n = 13) animals. *P<0.05. (**D**) Representative images of WGA (membrane; red) and DAPI (nuclear; blue) staining in left and right ventricular (epi: epicardial; endo: endocardial) and septal regions in transverse mid-ventricular heart sections from wild type and Kvβ2$^{-/-}$ animals. Scale bars = 25 μm. (**E**) and summary of

cardiomyocyte cross sectional area in regions as indicated in hearts from wild type and Kvβ2$^{-/-}$ animals. *P<0.05.

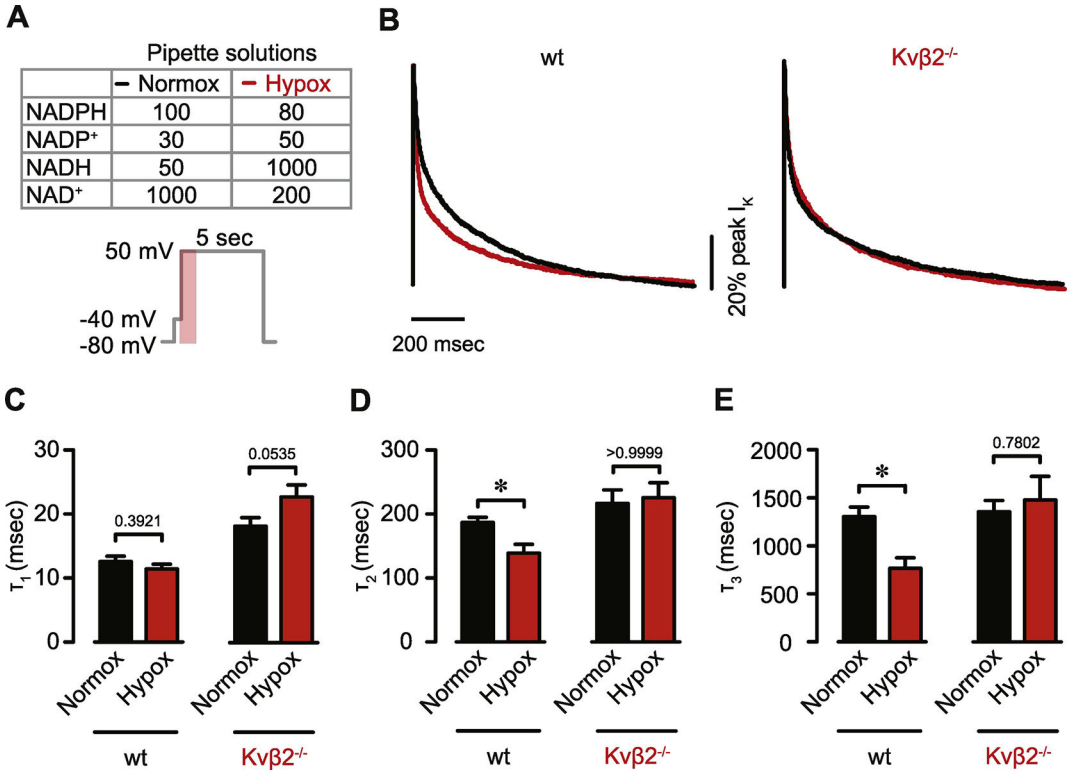

Figure 6: Modulation of cardiac myocyte I_{Kv} by intracellular pyridine nucleotide redox status.

(**A**) Table showing pyridine nucleotide concentrations (in μM) in pipette solutions used to reflect either normoxic or hypoxic conditions via intracellular dialysis (*top*) and voltage protocol (*bottom*). (**B**) Representative Kv currents in wild type and Kvβ2$^{-/-}$ myocytes (pA/pF, normalized to peak currents to show rate of decay between groups; period in shaded region of voltage protocol in A) after intracellular dialysis of normoxic and hypoxic pipette solutions (32°C). (**C**-**D**) Summary bar plots showing inactivation time constants (**τ**) obtained from tri-exponential fitting of voltage clamp recordings corresponding to I_{to} (τ_1), $I_{K,slow1}$ (τ_2) and $I_{K,slow2}$ (τ_3) for wild type and Kvβ2$^{-/-}$ myocytes in normoxic and hypoxic pyridine nucleotide conditions (n = 10–19 cells per condition). *P<0.01. ns: P>0.05.

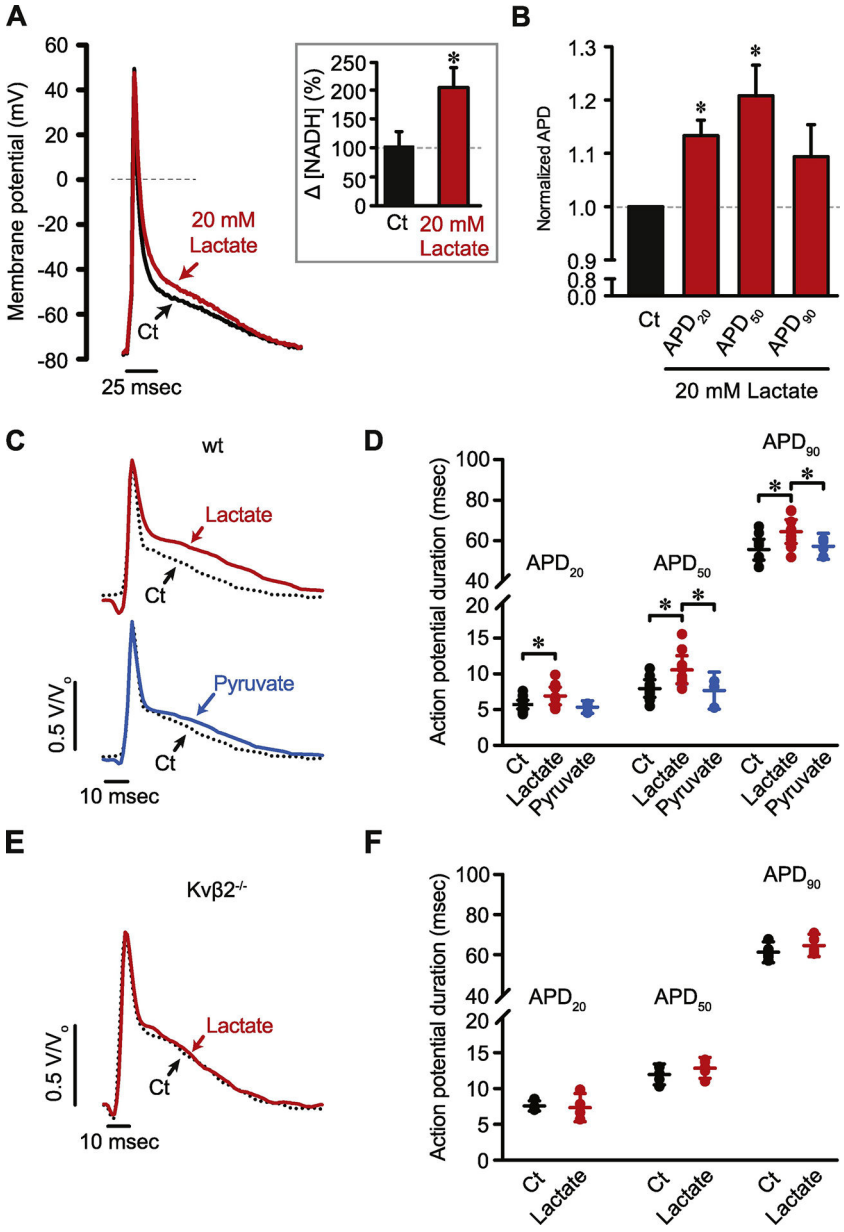

Figure 7: Lactate induced prolongation of the cardiac action potential requires Kvβ2.

(**A**) Representative perforated patch current clamp recordings of cellular action potentials in cardiac myocytes under control conditions (i.e., lactate-free) and 10 min after application of 20 mM lactate. (**A, *inset)*** Bar plot showing $[NADH]_i$ in hearts perfused with 20 mM lactate for 10 min (n = 5 hearts) relative to levels in hearts perfused with control (Ct) buffer for the same period of time (n = 4 hearts). (**B**) Bar plot showing action potential durations at 20%, 50%, and 90% repolarization 10 min after lactate relative to baseline control values (n = 6 cells). *P<0.05. ns: P>0.05. (**C**) Representative traces showing MAPs recorded in hearts from wild type (wt) animals in control (Ct) conditions and 10 min after application of 20 mM lactate (red trace) or 20 mM pyruvate (blue trace). (**D**) Scatter plot showing MAP durations at 20%, 50%, and 90% repolarization in hearts from wild type animals in Ct (n =

12 hearts), lactate (n = 9 hearts) and pyruvate (n = 4 hearts) conditions. (**E**) Representative traces showing MAPs recorded in hearts from Kvβ2$^{-/-}$ animals in control (Ct) conditions and 10 min after application of 20 mM lactate (red trace). (**F**) Scatter plot showing MAP durations at 20%, 50%, and 90% repolarization in hearts from Kvβ2$^{-/-}$ animals in Ct and after application of lactate (n = 5 hearts). *P<0.05.